Metal-Ligand Cooperation at Phosphine-Based Acceptor Pincer Ligands

Martine R. Tiddens and Marc-Etienne Moret

Contents

Abstract Acceptor ligands, which predominantly withdraw electron density from a transition metal center, often engage in weak metal-ligand interactions. These can be stabilized by flanking the acceptor moiety with strongly binding phosphines in a pincer motif, affording more robust complexes in which bond activation and/or bond-forming events can take place while preserving the integrity of the molecule as a whole. This contribution highlights recent developments in this area. Compounds incorporating a borane at the central position are discussed first, followed by compounds incorporating an electrophilic C = E (E = C, O, N) π-bond. In both cases, recent examples highlight the ability of these ligands to (1) respond to electronic changes at the metal by modifying their binding mode and (2) accept a

M. R. Tiddens and M.-E. Moret (✉)
Utrecht University, Organic Chemistry and Catalysis, Debye Institute for Nanomaterials
Science, Faculty of Science, Utrecht, The Netherlands
e-mail: M.Moret@uu.nl

nucleophilic fragment (e.g., hydride) from substrate molecules. Applications of acceptor pincer ligands as cooperative catalysts are discussed.

Keywords Acceptor ligands · Ambiphilic ligands · Bond activation · Cooperative catalysis · Metal-ligand cooperation · Pincer · π-Ligands

1   Introduction

The great successes of homogeneous catalysts in terms of stability, activity, and selectivity can be attributed to one's ability to precisely tune the properties of a transition metal (TM) center by means of ligand design. Traditionally, supporting ligands have been thought of as spectator ligands whose role was to tune the properties of a transition metal and thereby facilitate metal-centered bond activation of substrates. This paradigm is currently challenged by systems displaying metal-ligand cooperative reactivity, including (1) ligands facilitating bifunctional substrate activation [1–6], (2) redox-active ligands [7–14], and (3) ligands showing hemilabile coordination behavior [15–20]. Here, bond activation and/or bond-forming events involve strong interplay of the metal center and the cooperative ligand, facilitating reaction pathways that would be less accessible by using conventional homogenous catalyst. A prominent early example of catalysts incorporating bifunctional ligands is the BINAP/diamine-Ru system, where the amine ligand functions as a proton relay in the hydrogenation of ketones [21]. Since then, the metal amide/metal-amine interconversion has become one of the preeminent concepts for metal-ligand cooperative systems and has led to many catalytic applications [22, 23]. More broadly, ligands featuring a *donor* functional group that can transiently accept a proton or another electrophilic fragment now occupy a place of choice in the toolbox of synthetic chemists (and in the present volume).

More recently, cooperative ligands featuring an *acceptor* site for metal-ligand cooperation are emerging as a fertile area of investigations [24–31]. Whereas the classical description of coordination (Werner-type) and organometallic complexes involves ligands donating electron density to the metal, it had long been recognized that the bonding of many ligands (CO, olefins, and other π-ligands) could only be accurately described by including a secondary interaction involving electrons flowing from the metal to the ligand (π-backbonding). In the case of acceptor ligands, this inverse electron flow becomes the dominant bonding interaction: they feature an accessible empty orbital which forms a – generally weak – metal-ligand interaction by effectively withdrawing electron density from the transition metal. On the basis of the symmetry of the accepting orbital, a distinction between σ- or π-acceptor ligands can be made.

Acceptor ligands offer opportunities for unusual, cooperative bond activation pathways (Fig. 1). For instance, the accessible empty orbital of an acceptor ligand can act as a hydride relay in the bifunctional activation of E–H bonds or, more

Fig. 1 Cooperative processes at the weak metal-ligand interaction of a transition metal center (**M**) and an acceptor motif (**A**)
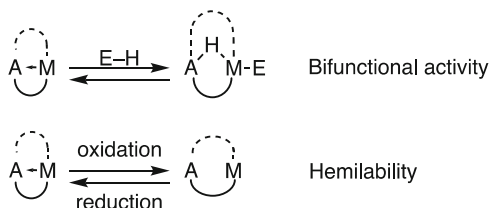
generally, reversibly accept a nucleophilic fragment. Furthermore, reversible coordination of the acceptor moiety can be expected to stabilize reduced intermediates in a catalytic cycle and hence accelerate the reaction.

However, these pathways would often cause the acceptor ligand or a derivative to (irreversibly) leave the coordination sphere of the metal, precluding catalysis. To overcome this limitation, an acceptor moiety can be flanked with strongly binding donor groups such as phosphines in the tradition of the original pincer design used to stabilize weaker TM–C bonds [32]. Pincer ligands generally afford robust complexes while leaving enough open space for incoming molecules to approach the reaction center [33–49]. Hence, *acceptor* pincer ligands can be expected to allow synergistic processes that preserve the integrity of the complex as a whole.

This chapter highlights recent examples of metal-ligand cooperation employing σ-acceptor (Sect. 2) and π-acceptor (Sect. 3) pincer ligands featuring P-donor tethers. Stoichiometric and catalytic cooperative processes are discussed, highlighting the unusual bond activation pathways enabled by *acceptor* pincer ligands. By comparing the reactivity of σ- and π-acceptor moieties, the similarities and differences of the synergistic processes they facilitate are highlighted.

2 σ-Acceptor Ligands

2.1 Ambiphilic Ligands and the Retrodative Bond Model

In his 1995 classification of covalent compounds of the elements [50], Green defines Z-type ligands as ligands that primarily accept electrons from the element they are bound to, i.e., Lewis acids. Transition metal complexes of such σ-acceptor ligands, however, remained merely scientific curiosities for a long time due to the scarcity of stable examples. In the context of coordination chemistry and catalysis, Lewis acids were mostly used as external activators, co-catalysts, or additives. The field emerged as an area of systematic investigation when the group of Hill reported the first fully characterized metallaboratrane in 1999 (Fig. 2, left) [51] in which a trisubstituted borane is the σ-acceptor moiety. A hydrido-borate scorpionate ligand was shown to react with Ru^{II} vinyl precursors via B–H addition to form a supported Ru→B interaction. This initial discovery prompted systematic investigations of TM→B bonds supported by scorpionate ligands featuring sulfur- and nitrogen-based buttresses which are covered in several interesting reviews [24, 27, 29].
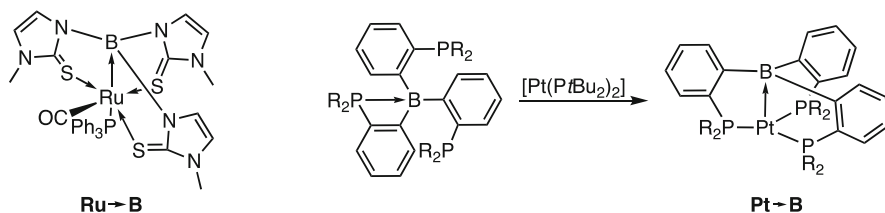
Fig. 2 Ruthenaboratrane reported by Hill and co-workers in 1999 (left) [51] and the Pt^0 complex of Bourissous' trisphosphinoborane ligand (right) [52]
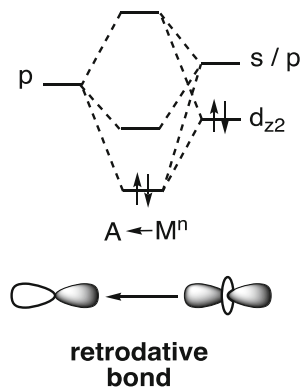

Fig. 3 Schematic representation of a retrodative bond formation by donation of electron density from a transition metal orbital to the empty p-orbital of a σ-acceptor ligand and molecular orbital diagram for the retrodative bond formation

A second, more versatile approach to the formation of a weak TM→A interaction (A = acceptor) relies on the synthesis of ambiphilic ligands combining Lewis basic site(s) and Lewis-acidic site(s): a field pioneered by Bourissou and co-workers [53]. Figure 2 (right) shows the ambiphilic triphosphine-borane ligand featuring an intramolecular P→B bond, which is in equilibrium with its open form [54]. Coordination of this tetradentate ligand to Pt^0 readily affords a cage structure with intrinsic C_3 symmetry [52]. In general, ambiphilic ligands offer relatively straightforward and reliable access to complexes featuring a TM→A interaction, and while the most commonly used Lewis-acidic center is boron, ligands featuring heavier group 13 or group 14 elements as σ-acceptor moiety have been reported on. Their coordination chemistry and reactivity have been discussed in recent reviews [24, 26, 31].

As this new research area of σ-acceptor ligands developed, it led to a better understanding of the proposed underlying bonding model for a TM→A interaction. In general, in the coordination of a σ-acceptor ligand, the metal acts primarily as Lewis base. A so-called retrodative bond of σ-character is formed between a filled metal orbital and the accessible empty orbital of the σ-acceptor ligand (Fig. 3). The electron-withdrawing effect of the retrodative bond stabilizes the filled metal orbital. In addition, a second bonding combination is formed between one empty metal
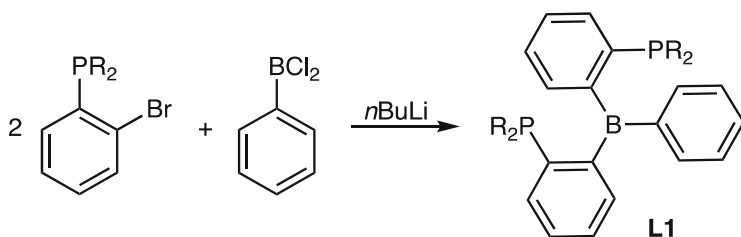
Scheme 1 Synthesis of **L1** with R = *i*Pr or Ph; according to Bourissou and co-workers [56]

orbital of s or p parentage and the σ-acceptor. This low-lying vacant orbital is responsible for an increased Lewis acidity of TM→A complexes [55].

Depending on the number of donor buttresses introduced in the ambiphilic ligand, flexible or more rigid structures are obtained from mono-, bi-, or tripodal ligand frameworks. In particular, the pincer-like bipodal framework offers a good compromise between stability and reactivity: this design strongly anchors the boron atom in the vicinity of the metal center without excessively shielding it from reagent molecules. Hence, the formed weak TM→B interaction bears potential for metal-ligand cooperative reactivity.
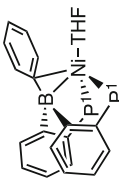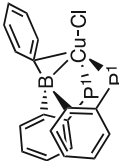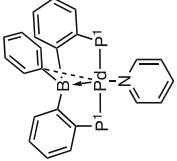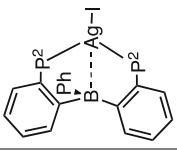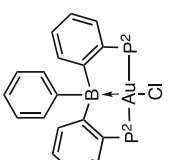
Phosphine-tethered borane ligands of type **L1** (Scheme 1) were first synthesized by Bourissou and co-workers via a lithium/halogen exchange between *o*-diphenylphosphino-bromobenzene and dichlorophenylborane (for R = Ph) [56]. The use of **L1** type ligands has proven a fruitful strategy to study the TM→B (B = borane) retrodative bond as it potentially coordinates κ³ (P,B,P) to a transition metal center with a retrodative bond between the metal and the boron center. In the following, the coordination chemistry of **L1** to late transition metal centers and the reactivity of the resulting complexes are briefly discussed, and illustrative examples of metal-ligand cooperative catalysis are presented.

2.2 Metal-Ligand Cooperative Catalysis Employing d^{10} Complexes of the σ-Acceptor Ligand Diphosphinoborane

The borane ligand **L1** is designed to support a TM→B interaction. Table 1 shows a selection of d^{10} complexes featuring such a retrodative bond. The tetrahedral complex **L1Ni⁰(THF)** was reported by Peters and co-workers to feature a $\eta^2(B,C_{ipso})$ coordination rather than the expected $\eta^1(B)$ interaction, meaning that the Ni→B interaction is supported by arene coordination (Table 1) [57]. This binding mode is characterized by short TM–B and TM–C_{ipso} distances and a relatively low pyramidalization of the boron atom.

The isoelectronic **L1Cu⁰Cl** structure also adopts a tetrahedral geometry featuring a similar arene-supported $\eta^2(B,C_{ipso})$ coordination (Table 1), but a longer TM–B bond distance of Cu–B = 2.396(5) Å [58]. Bourissou and co-workers proposed the

Table 1 The different d^{10} complexes of **L1** adopt different overall geometries with TM→B retrodative bond interactions of different strengths (THF = tetrahydrofuran, ΣB_α = sum of angles around boron) [57–61]

Ni–B: 2.124(2) Å	Cu–B: 2.396(5) Å	Pd–B: 2.194(3) Å	Ag–B: 2.742(3) Å	Au–B: 2.309(8) Å
Ni–C$_{ipso}$: 2.175(2) Å	Cu–C$_{ipso}$: 2.364(3) Å	Pd–C$_{ipso}$: 2.463(3) Å	Ag–C$_{ipso}$: 2.939(3) Å	Au–C$_{ipso}$: 3.099(8) Å
ΣB_α: 352°	ΣB_α: 356°	ΣB_α: 346°	ΣB_α: 357°	ΣB_α: 341°
P^1 = PPh$_2$	P^1 = PPh$_2$	P^1 = PPh$_2$	P^2 = PiPr$_2$	P^2 = PiPr$_2$

presence of a three-center Cu–B–C$_{ipso}$ interaction on the basis of Kohn-Sham orbitals obtained by density functional theory (DFT) calculations. Natural bond orbital (NBO) analysis showed that among the various donor-acceptor interactions involving this triangle, a Cu→B donating interaction of similar magnitude as the η^1(B) interactions found in related complexes is present [24]. Additionally, natural population analysis confirms a net charge transfer from Cu to B, reinforcing the description of the ligand as an acceptor ligand.

Moving to the second and third row transition metal centers, **L1** coordinates to Au^I in an initially unexpected yet most pincerlike manner [61]. A square planar geometry around the tetracoordinated Au^I is observed, featuring *trans*-diphosphine coordination of **L1** and a chloride co-ligand *trans* to the η^1(B)-coordinated borane (Table 1). A strong Au→B interaction is observed as evident from a short bond distance (2.309(8) Å) and strong pyramidalization of the borane center (ΣB$_\alpha$ = 341°). Frontier orbital analysis shows a B–Au–Cl three-center interaction; however, the charge depletion at gold and charge increase at boron are not large enough to be considered a 2e$^-$ oxidation of the gold center to Au^{III}. In addition, ^{197}Au Mössbauer spectroscopy supported the classification of **L1Au^{I}Cl** as a 16 VE Au^I complex.

The distinct η^1(B) and arene-supported η^2(B,C) coordination modes can be considered two extremes of **L1** coordination to d^{10} transition metal centers. This becomes apparent upon the evaluation of the coordination of **L1** to Pd^0 [59]. Depending on the donor strength and steric requirements of the phosphine tethers, the Pd complexes of **L1** adopt a strongly distorted square planar geometry (P^1 = PPh$_2$, Table 1) with at most a weak Pd–C$_{ipso}$ interaction (Pd–C = 2.463(3) Å) or a T-shape geometry (P^3 = PCy$_2$, Cy = cyclohexyl, no co-ligand) [62]. Both complexes feature a strong Pd→B interaction as evident from short Pd–B bond distances (Pd–B = 2.194(3) Å for P^1 = PPh$_2$ and Pd–B = 2.243(2) Å for P^3 = PCy$_2$) and a significant pyramidalization of the boron atom (ΣB$_\alpha$ = 346° for P^1 = PPh$_2$ and ΣB$_\alpha$ = 341° for P^3 = PCy$_2$).

In contrast with other d^{10} analogues, the silver(I) complex **L1Ag^I(I)** exhibits a very weak TM→B interaction (Table 1) [60]. Rather than κ^3 (P,B,P), a trigonal planar κ^2 (P,P) coordination geometry was proposed based on the sum of angles of 356.5° in the P$_2$AgI plane. Competing B–F bond formation prevents the coordination of **L1** to AgF, showing that halide abstraction can hamper coordination of σ-acceptor ligands.

This study of **L1** coordination to d^{10} transition metals nicely illustrates how acceptor ligands can give rise to structures that challenge our understanding of the bonding and geometry of transition metal complexes. More generally, the series of complexes shown in Table 1 exposes the coordination flexibility of the **L1** platform, demonstrating most importantly that the TM–B interaction is not enforced by the pincer architecture but rather a possibility among several accessible geometries.

Inagaki and co-workers hypothesized that the electron-depleting nature of **L1** would amplify the intrinsic alkynophilicity of a gold cationic center which, in catalysis, can be utilized for a more effective activation of alkynes towards nucleophilic attack. For this purpose, cationic Au^I complexes of **L1** were synthesized (Scheme 2) [63]. The synthesis of an **L1Au$^+$** fragment from **L1Au^{I}Cl** by direct
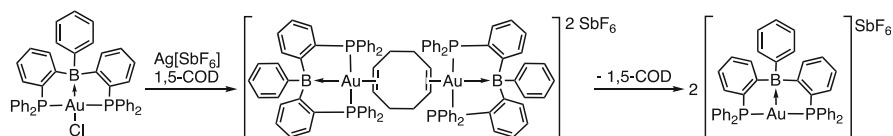
Scheme 2 Synthesis of the cationic **[L1Au][SbF$_6$]** complex by indirect halide abstraction; 1,5-COD = 1,5-cyclooctadiene [63]

halide abstraction proved difficult. Therefore, a dinuclear species stabilized by a 1,5-cyclooctadiene (1,5-COD) bridge, **[(L1Au)$_2$(COD)][SbF$_6$]$_2$** (Scheme 2, middle), was obtained first by using Ag[SbF$_6$] in the presence of 1,5-COD. During crystallization, the 1,5-COD co-ligand dissociates to afford the mononuclear **[L1Au][SbF$_6$]** species, which was characterized by X-ray crystallography.

The Au→B bond is significantly weakened by halide abstraction as evident from an elongated Au–B distance of 2.52(1) Å in **[L1Au][SbF$_6$]** vs 2.335(5) Å in **L1Au^{I}Cl**. In addition, the sum of C–B–C angles increases from 344° to 355.1°, indicating a boron hybridization close to sp^2. The other bond distances and angles do not undergo major changes, showing that the electron density at the Au$^+$ center has a direct influence on the TM→B bond strength.

The cationic gold species was tested as catalyst for the cycloisomerization of enynes, in which alkyne activation by coordination to the gold center is followed by an intramolecular nucleophilic attack. In their recent "digest paper" [64], Inagaki and co-workers discuss seven examples in which the presence of a retrodative bond between the gold cation and the σ-acceptor **L1** leads to a higher catalytic activity and selectivity. Table 2 shows the [2+2] cycloaddition of 1,8-enynes as an example of these comparative studies. The dinuclear species **[(L1Au)$_2$(COD)][SbF$_6$]$_2$** was used as precatalyst. Under the optimized reaction conditions of 2 mol% [Au$^+$] in 1,2-dichloroethane (DCE) at room temperature for 24 h, a seven-membered ring was selectively formed in moderate to good yields depending on the substitution. Directly compared to other phosphine-stabilized gold cations such as [(PPh$_3$)$_2$Au] [SbF$_6$], [(PPh$_3$)Au][SbF$_6$], [(XPhos)Au][SbF$_6$], or [(Xantphos)Au][SbF$_6$] (Table 2), the **[L1Au)$_2$(COD)[SbF$_6$]$_2$** species shows superior catalytic activity indicating that the TM→B interaction has a beneficial effect on the reactivity of the gold cation.

While no in-depth mechanistic study was conducted, it is assumed that a σ-acceptor *trans* to the triple bond induces an electron push-pull charge transfer across the alkyne–Au→B coordination plane by donation of more electron density into the Au→B bond. This results in a stronger activation of the triple bond and subsequently facilitates nucleophilic attack by the olefin. Overall, this study serves as an example of metal-ligand cooperative catalysis in which the weak and responsive TM→B interaction is utilized to enhance the Lewis acidity of the transition metal center.

Peters and co-workers demonstrated how the accessible empty orbital of **L1** can be used as hydride relay in bifunctional dihydrogen (H$_2$) activation and catalytic reduction of olefins [57, 65]. The initial **L1Ni^0(THF)** complex (Table 1) appeared unreactive towards H$_2$, suggesting the cleavage of the η^2(B,C$_{ipso}$) coordination to be

Table 2 Comparative study of the [Au$^+$] catalyzed [2+2] cycloaddition of 1,8-enynes; DCE = dichloroethane, Ar = argon atmosphere [63]
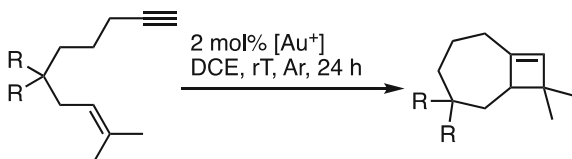

[Au$^+$]	Substrate	Yield
2 SbF$_6$	R = CO$_2$Me	62%
	R = CH$_2$OPiv	85%
[PPh$_3$–Au–PPh$_3$]SbF$_6$	R = CO$_2$Me	No reaction
	R = CH$_2$OPiv	No reaction
[PPh$_3$–Au]SbF$_6$	R = CO$_2$Me	16%
	R = CH$_2$OPiv	51%
SbF$_6$	R = CO$_2$Me	No reaction
	R = CH$_2$OPiv	No reaction
SbF$_6$	R = CO$_2$Me	39%
	R = CH$_2$OPiv	55%

difficult. The exchange of the phosphine substituents in **L1** from phenyl to isopropyl, however, enabled the isolation of a dinitrogen complex **L1Ni^0(N$_2$)**, which upon addition of H$_2$ gas exchanges ligands to form a nonclassical Ni–(H$_2$) adduct (Scheme 3) [65]. Over the course of several hours, the formation of a bridging borohydride–Ni–hydride complex was observed by NMR.

During H$_2$ activation, the nature of the Ni→B interaction changes from a modest perturbation exerted by the empty p(B) orbital on the d^{10}(Ni) center bearing a σ-bound H$_2$ ligand to the interaction of an anionic borohydride ligand stabilizing the mononuclear Ni^{II}–H species. While *cis* homolytic H$_2$ activation via a *cis*-dihydride intermediate cannot be fully ruled out, computational studies conclude that synergetic heterolytic H$_2$ activation is the most likely mechanism [66]. No high-
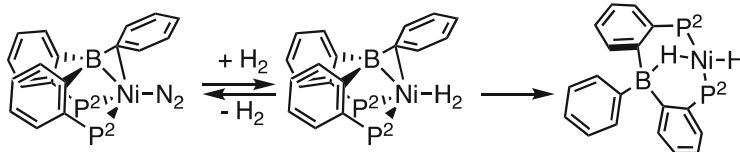
Scheme 3 Synthesis of a nonclassical Ni–(H$_2$) adduct by N$_2$/H$_2$ exchange at **L1Ni^0(N$_2$)** and bifunctional H$_2$ activation across the Ni→B interaction to form a bridging borohydride–Ni–hydride species; P^2 = PiPr$_2$ [65]
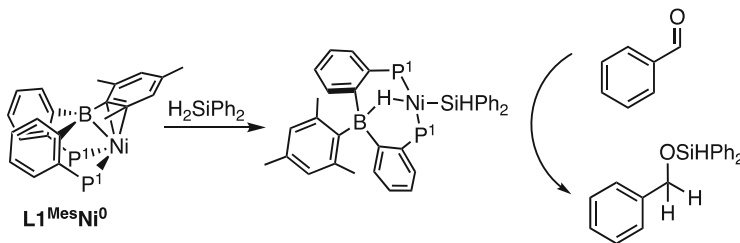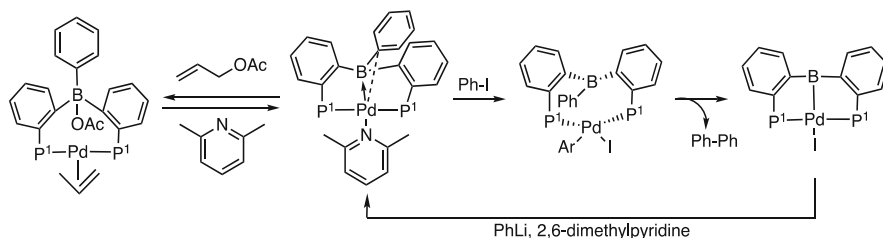

Scheme 4 Bifunctional activation of the Si–H bond in diphenylsilane across the Ni→B interaction enables the catalytic hydrosilylation of benzaldehyde; P^1 = PPh$_2$ [67]

energy penalty seems to be associated with breaking the Ni→B interaction in this process.

Experimentally, H$_2$ activation was shown to be more facile using a slightly altered **L1**Ni-system where a mesityl group replaces the phenyl group on boron (**L1^{Mes}Ni^0**, Scheme 4) [57]. Hereby, steric bulk likely weakens the Ni→B interaction, which becomes a η^3(B,C,C) coordination involving the *ipso* and *ortho* carbon of the mesityl substituent. The resulting **L1^{Mes}Ni^0** complex undergoes facile and instantaneous reaction with H$_2$ to form the bridging borohydride–Ni–hydride species. Using this **L1^{Mes}Ni^0** complex, catalytic styrene hydrogenation under very mild conditions (4 atm H$_2$) was observed, constituting an example of bifunctional H$_2$ activation involving a σ-acceptor ligand in a catalytic reaction. Additionally, stoichiometric reaction of **L1^{Mes}Ni^0** with diphenylsilane (H$_2$SiPh$_2$) shows the formation of a bridging borohydride–Ni–(SiHPh$_2$) species resulting from the bifunctional activation of the Si–H bond over the Ni→B interaction (Scheme 4) [67].

The solid-state structure of the bridging borohydride–Ni–(SiHPh$_2$) supports the structural analysis of the bridging borohydride–Ni–hydride species, which was so far based on NMR analysis alone. Si–H bond activation leads to a Ni^{II} center which adopts a distorted square planar geometry. The η^3(B,C,C) interaction is broken as the mesityl group decoordinates to accommodate the bridging hydride. Furthermore, a Ni–Si bond distance of 2.2435(7) Å is found supporting the Ni–silyl characterization. Under mild catalytic conditions, the **L1^{Mes}Ni^0** complex is a competent catalyst in the hydrosilylation of benzaldehydes with H$_2$SiPh$_2$ (Scheme 4). Here as well, it is proposed that the borane σ-acceptor functions as hydride relay in this metal-ligand cooperative catalytic transformation.

Scheme 5 Bifunctional activation of allyl acetate across the Pd→B interaction (left) [59] and conversion of a σ-acceptor borane ligand into a σ-donor boryl ligand by phenyl group transfer (right); $P^1 = PPh_2$ [68]

Tauchert and co-workers studied oxidative addition at the **L1Pd⁰(2,6-lutidine)** complex [59]. No reactivity towards bromobenzene was observed. However, a reaction with iodobenzene leads to the classic oxidative addition product which over time undergoes a reductive elimination of the phenyl-substituent on boron and the phenyl-ligand on Pd^{II} leading to a PBP–Pd^{II} boryl pincer complex (Scheme 5, right) [68]. The reaction of this complex with phenyl lithium in the presence of 2,6-lutidine gives back the starting **L1Pd⁰(2,6-lutidine)** complex. Overall, this phenyl group transfer enables the reversible conversion of a σ-acceptor borane ligand to a σ-donor boryl moiety, which is one promising strategy to access transition metal boryl complexes [69].

The Pd→B retrodative bond depletes electron density at the Pd center, thereby impeding activation of strong σ-bonds via classical oxidative addition. Therefore, bifunctional C–O bond activation across the Pd→B interaction was attempted by Tauchert and co-workers in a reaction of the **L1Pd⁰(2,6-lutidine)** complex with allyl acetate (Scheme 5, left) [59]. Here, a Pd-allyl complex and a new B–OAc bond are formed. C–O bond activation is thought to be favored by the formation of a new strong B–O bond, showing that the σ-acceptor borane can function as relay for other groups than hydrides.

The allyl acetate activation is reversible, and the equilibrium can be shifted by addition of 2,6,-lutidine (Scheme 5, left). This reactivity was applied in the catalytic allylic substitution reaction of allyl acetate with diethylamine. However, an accelerating effect of added tetrabutylammonium acetate suggests that species featuring a strong Pd→B interaction may be inactive, the extra acetate source breaking the Pd→B bond and thereby enhancing Pd-centered catalytic conversion.

Recently, Kameo and Bourissou reported a different cooperative approach to facilitate the activation of strong σ-bonds, specifically of aromatic C–Cl bonds, using **L1Pd⁰(PPh₃)**. While **L1** coordination results in the depletion of electron density at the Pd center of **L1Pd⁰(PPh₃)**, a more electron-rich Pd species is formed in a subsequent reaction with potassium hydride (KH). Here, a hydride insertion into the Pd→B bond forms a B–H–Pd bridge in the overall anionic Pd complex **K[L1-H-Pd(PPh₃)]** [70]. This hydride is positioned at the apical position in an overall trigonal-pyramidal geometry at the Pd center (Fig. 4).
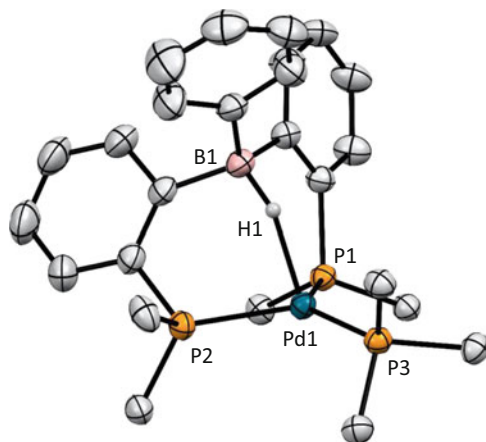
Fig. 4 X-ray crystal structure of **K[L1-H-Pd(PPh₃)]** showing the bridging borohydride motif (thermal ellipsoids at 50% probability). The [K([2.2.2]-cryptand)] cation, hydrogen atoms (except the borohydride), and phenyl groups on the phosphorus atoms (except for the bound carbon atom) are omitted for clarity [70]
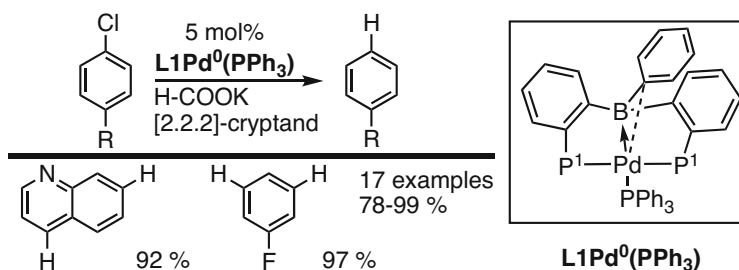

Fig. 5 Catalytic hydrodechlorination of (hetero)aryl chlorides (reaction conditions: 60–100°C, 48–72 h); $P^1 = PPh_2$ [70]

The electron-rich **[L1-H-Pd(PPh₃)]K** is reactive towards various C–Cl bonds, which was used in the catalytic hydrodechlorination of (hetero)aryl chlorides (Fig. 5). In this system, potassium formate is used as hydride source. High yields and a high functional group tolerance were observed for heteroarene substrates. Lower yields were obtained for substrates featuring electron-donating substituents *para* to the C–Cl bond, in line with the general trend of oxidative addition being more difficult when the C–Cl bond is less polarized.

Based on computational work, a catalytic cycle for hydrodechlorination was proposed (Fig. 6). In contrast with the general Pd-catalyzed C–C cross-coupling mechanism, which consists of a sequence of oxidative addition, transmetalation, and reductive elimination, this reaction starts by reaction of **L1Pd⁰(PPh₃)** with KH to form the anionic Pd⁰ borate **[L1-H-Pd(PPh₃)]⁻**, which then undergoes oxidative addition of the C–Cl bond and elimination of KCl to form a proposed Pd–Ar
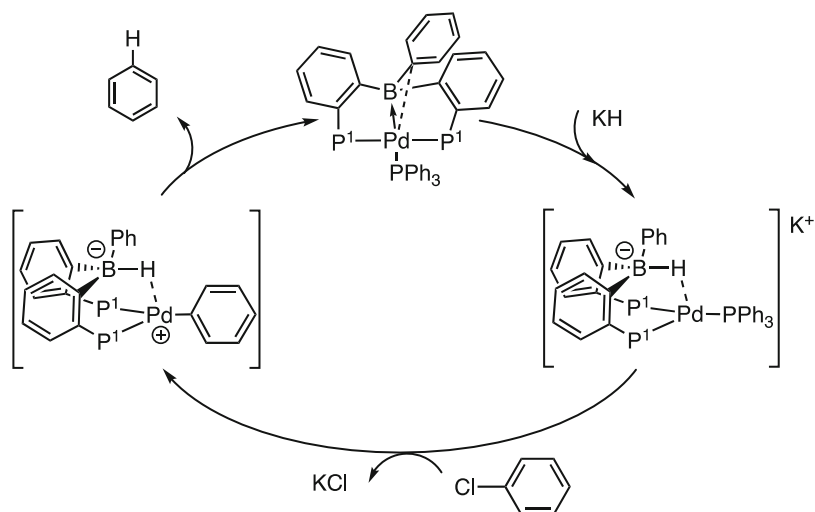
Fig. 6 Proposed catalytic cycle for the catalytic hydrodechlorination of (hetero)aryl chlorides; $P^1 = PPh_2$ [70]

intermediate. The following B-to-Pd hydride transfer and reductive elimination of the C–H bond are exergonic and most likely facilitated by the formation of a TM→B interaction.

2.3 Metal-Ligand Cooperative Reactivity at Group 8 and 9 Complexes of the σ-Acceptor Ligand Diphospinoborane

As low spin d^8 transition metal complexes tend to adopt a square planar geometry, their filled d_{z2} orbital might act as Lewis base to an apical σ-acceptor moiety in an overall square pyramidal complex. Such a TM→B interaction is observed in the 16VE **L1Rh^{I}Cl(DMAP)** complex featuring a 4-dimethylaminopyridine (DMAP) co-ligand (Fig. 7) [56]. Indeed, the Rh center adopts a square pyramidal geometry with the boron atom in the apical position to maximize the orbital overlap between the full d_z^2(Rh) orbital and the empty p(B) orbital. NBO calculations find a two-center two-electron (2c2e) bond between Rh and B. A strong TM→B interaction is evident from the pyramidalized boron center ($\Sigma B_\alpha = 340.2°$) and a short Rh–B distance (2.295(5) Å). In addition, the ^{11}B NMR signal shifts upfield to 19.4 ppm from 43 ppm in **L1**, indicating a four-coordinate boron atom. The geometry of **L1Rh^{I}Cl(DMPA)** is representative for low spin d^8 TM complexes of **L1** (Fig. 7). Bourissou and co-workers evaluated the variety in TM→B interaction strength in Rh^I, Pt^{II}, and Pd^{II} complexes of **L1** specifically. Based on ^{11}B NMR and X-ray data, the study revealed the TM→B interaction to become significantly weaker when going from Rh^I to Pt^{II} to Pd^{II}. Therefore, this series of d^8 complexes of **L1** illustrates
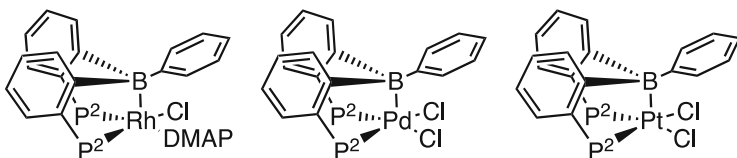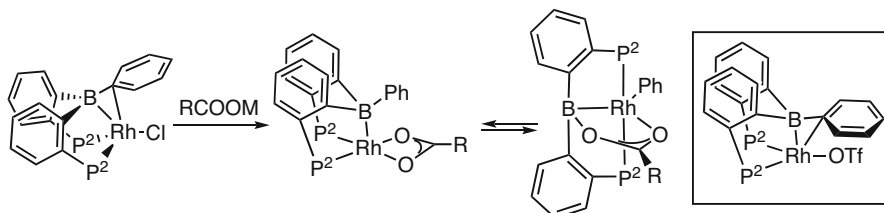
Fig. 7 Square pyramidal d^8 complexes of **L1**; DMAP = 4-dimethylaminopyridine, $P^2 = PiPr_2$


Scheme 6 Reaction of **L1Rh^{I}Cl** with bidentate oxygenous ligands (RCOOM = KOAc, CsOPiv). The phenyl group transfer from B to Rh is an equilibrium which is proposed to go through an intermediate species featuring a $\eta^2(B,C_{ipso})$ coordination mode of **L1** similar to the isolated species (box) from a reaction of **L1Rh^{I}Cl** with TMSOTf; $P^2 = PiPr_2$ [72]

how the coordination strength of the σ-acceptor borane to the transition metal center is a continuum tuned by the intrinsic Lewis basicity of the metal center.

The Lewis acidity of the central boron atom in **L1** is quenched by coordination to a transition metal center as was experimentally shown by Britovsek and co-workers. They attempted bifunctional C–O bond activation across a Rh→B interaction in the reaction of square pyramidal **[L1Rh^I(CO)$_2$][SbF$_6$]** species with methyl acetate [71]. In contrast with the related **L1Pd^0(2,6-lutidine)** complex (Scheme 5, Sect. 2.2), **[L1Rh^I(CO)$_2$][SbF$_6$]** is unreactive towards neutral oxygen-containing substrates, which was attributed to the strong Rh→B interaction.

Ozerov and co-workers later reported on the reactivity of **L1Rh^{I}Cl** species with anionic oxygen-containing substrates (Scheme 6). A borane-to-boryl interconversion by phenyl transfer from the ligand to the transition metal center was observed upon the reaction with alkali-metal carboxylates [72]. Two isomers are observed in equilibrium upon a reaction of **L1Rh^{I}Cl** with potassium acetate (KOAc) or cesium pivalate (CsOPiv). The initial replacement of chloride results in a Rh species featuring a Rh→B interaction and a κ^2-carboxylate co-ligand. The second species features a terminal phenyl group on Rh and a sp^3-hybridized borate ligand with a carboxylate bridge between Rh and B. This bridging interaction is not present in the product of the reaction of **L1Rh^{I}Cl** with trimethylsilyl triflate (TMSOTf). Instead, a $\eta^2(B,C)$ coordination of **L1** is observed (Scheme 6, box). Most likely, the lower Lewis basicity of triflate does not allow for B–O adduct formation. A related species featuring a $\eta^2(B,C)$ interaction was proposed to be an intermediate along the reaction pathway of the phenyl group transfer process.

Across the periodic table, the bridging borohydride (B–H–TM) motif seems to be broadly accessible to transition metal complexes of **L1**. Kameo and Nakazawa
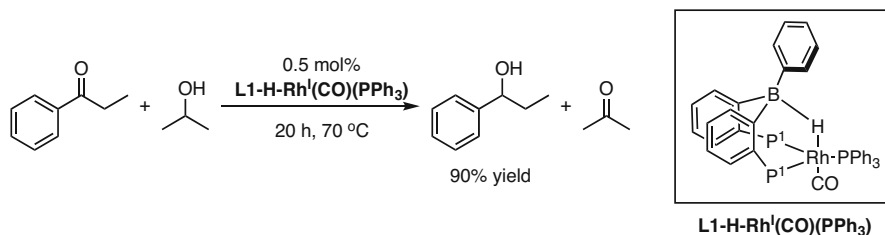
Scheme 7 Reaction scheme of a transfer hydrogenation catalyzed by the **L1-H-Rh^I(CO)(PPh$_3$)** featuring a bridging borohydride motif; P^1 = PPh$_2$ [73]
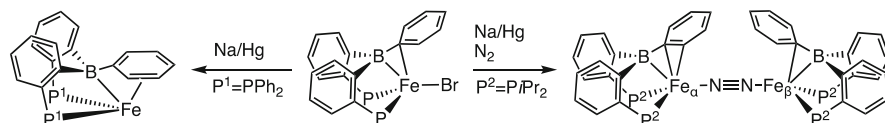

Scheme 8 Reduction of **L1Fe^{I}Br** by one electron results in the case of P^1 = PPh$_2$ in a **L1Fe^0** complex featuring a η^7(B,Ph) coordination (left), whereas P^2 = PiPr$_2$ leads to a dinuclear N$_2$ bridged **L1Fe(μ-1,2-N$_2$)FeL1** complex featuring one η^3(B,C$_{ipso}$,C$_{ortho}$) and one η^2(B,C$_{ipso}$) coordination mode of **L1** (right) [74]

reported a **L1-H-Rh^I(CO)(PPh$_3$)** species (Scheme 7) synthesized from the reaction of **L1** with Rh(H)(CO)(PPh$_3$)$_3$ [73]. Structurally, the B–H–Rh species resembles the anionic **[L1-H-Pd(PPh$_3$)]K** species (Sect. 2.2, Fig. 6) [70]: in the solid state, the Rh center adopts a trigonal-bipyramidal geometry with a hydride at the apical position. This hydride is part of an overall three-center two-electron (3c2e) B–H–Rh interaction. This bonding interaction was further analyzed by NBO comparative analysis of the free ligand (**L1**), the Rh(H)(CO)(PPh$_3$)$_3$ precursor, and the **L1-H-Rh^I(CO)(PPh$_3$)** species. While the charge on boron increases and the charge on Rh decreases as expected upon coordination of **L1** to the Rh precursor, the B–H–Rh interaction seems to minimally influence the charge on the hydride, suggesting that the σ-acceptor effectively withdraws electron density from the transition metal center via the B–H–TM motif.

L1-H-Rh^I(CO)(PPh$_3$) is a catalyst for the transfer hydrogenation of propiophenone with isopropanol (Scheme 7) [73]. Though the mechanism of this catalytic reaction was not further studied, **L1-H-Rh^I(CO)(PPh$_3$)** outcompetes the boron-free Rh(H)(CO)(PPh$_3$)$_3$ species in catalytic activity significantly (90% yield versus 29% yield) indicating a positive influence of the **L1** coordination.

First-row d^8 transition metal complexes of **L1** were reported by Peters and co-workers as they synthesized the **L1Fe^{I}Br** complex from in situ reduction of FeBr$_2$ in the presence of **L1**, showing the propensity of borane ligands to stabilize Fe^I species [74]. An extra one-electron reduction led to the formation of the dinuclear N$_2$-bridged complex **L1Fe(μ-1,2-N$_2$)FeL1** (P^2 = PiPr$_2$, Scheme 8, right) or a η^7(B,Ph)-coordinated monomeric **L1Fe^0** species (P^1 = PPh$_2$, Scheme 8, left).

The peculiar η^7(B,Ph) mode is achieved by distorting the B–C$_{ipso}$ bond in **L1**. The higher hapticity in the diamagnetic Fe complex is maintained in solution according
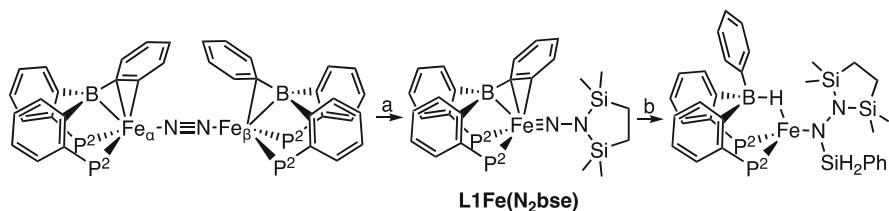
Scheme 9 N_β functionalization by reaction of **L1Fe(μ-1,2-N$_2$)FeL1** with (**a**) 1,2-bis (chlorodimethylsilyl)ethane and 2.1 equivalent Na/Hg to form **L1Fe(N$_2$bse)** and N_α functionalization upon a subsequent hydrosilylation with (**b**) PhSiH$_3$, P^2 = PiPr$_2$ [74]
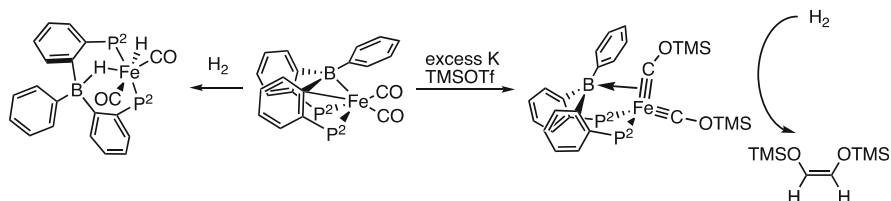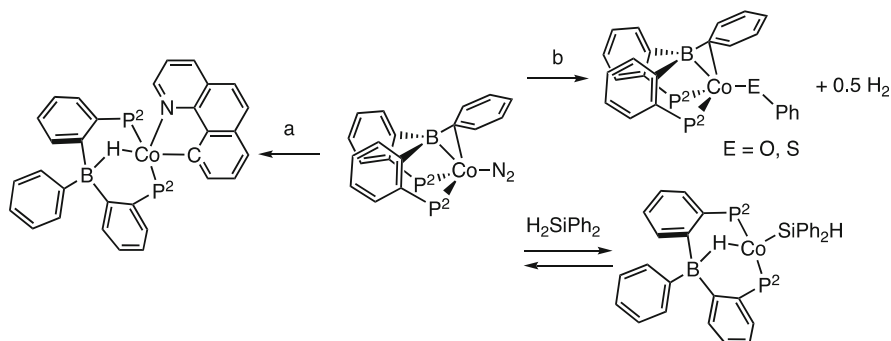

Scheme 10 Bifunctional H$_2$ activation across the Fe→B bond (left) and iron dicarbyne synthesis by oxygen atom functionalization with trimethylsilyl triflate (TMSOTf). Addition of 1 atm H$_2$ leads to the formation of an olefin product: P^2 = PiPr$_2$, K = potassium [75]

to the upfield shift of aryl resonances in ^{1}H NMR. In the dinuclear species, the pseudotetrahedral Fe centers are inequivalent as Fe$_\alpha$ coordinates **L1** η^3(B,C$_{ipso}$, C$_{ortho}$), whereas the Fe$_\beta$ shows a η^2(B,C$_{ipso}$) coordination. In solution, however, the Fe centers are equivalent, leading to assumption that the η^3(B,C,C) interaction is highly flexible, which makes these Fe species ideal starting points of further studies into metal-ligand cooperative reactivity.

The Fe-bound N$_2$ molecule was functionalized at the N$_\beta$ position in the reaction of **L1Fe(μ-1,2-N$_2$)FeL1** with 1,2-bis(chlorodimethylsilyl)ethane and 2.1 equivalents of Na/Hg to form the iron-aminoimide complex **L1Fe(N$_2$bse)** (Scheme 9, middle) [74].

The double silylation of N$_\beta$ results in a pseudotetrahedral d^6 Fe-aminoimide complex featuring a η^3(B,C,C) interaction as well as a Fe $\equiv$ N triple bond (Fe–N, 1.6607(5) Å) and a reduced N–N bond (N–N bond distance average, 1.326 Å). As the TM→B interaction was shown to activate H–E bonds (E = H, Si) in a bifunctional manner (Sect. 2.2), **L1Fe(N$_2$bse)** was reacted with phenylsilane (PhSiH$_3$) in an attempt to hydrosilylate the Fe $\equiv$ N triple bond. A facile reaction results in silylation at Nα, whereas the hydride is incorporated into a B–H–Fe motif (Scheme 9, right). The iron hydrazido species features a N–N bond distance of 1.492(4) Å indicating a single bond. Hence, in the overall two-step reduction of a N$_2$ triple bond to a single bond, the σ-acceptor ligand **L1** acts both as a stabilizing ligand for an electron-rich Fe^0 center and as a hydride acceptor in the bifunctional hydrosilylation of the Fe $\equiv$ N triple bond.

Upon addition of 1 atm CO to **L1Fe(μ-1,2-N$_2$)FeL1**, the mononuclear iron dicarbonyl species **L1Fe(CO)$_2$** was formed (Scheme 10, middle) [75]. The iron dicarbonyl species features a Fe→B retrodative bond and an interaction between

Scheme 11 Bifunctional C–H bond activation (left) and reactivity of **L1Co⁰(N₂)** with E–H (E = O, S, Si) bonds (right), (**a**) benzoquinoline and (**b**) phenol or thiophenol; $P^2 = PiPr_2$ [76]

iron and one phenylene linker. Facile H_2 activation by **L1Fe(CO)₂** with 1 atm H_2 leads to the formation of a bridging B–H–Fe motif as well as a Fe–H bond (Scheme 10, left). X-ray analysis reveals *cis*-dihydride stereochemistry.

Double oxygen atom functionalization was observed in a reaction of **L1Fe(CO)₂** with TMSOTf under strongly reducing conditions (excess potassium; Scheme 10). The disilylation results in a structurally unique iron dicarbyne complex in which the Fe→B interaction is replaced by a stabilizing $(Fe≡C_{carbyne})→B$ interaction. This interpretation of the bonding situation is based on a relatively long Fe–B distance (2.593(1) Å) and shorter $C_{carbyne}$–B distance (1.862(1) Å) obtained from the X-ray crystal structure. Additionally, the boron atom is pyramidalized ($\Sigma B_\alpha = 328°$), indicating borate character. Facile C–C bond formation is observed upon the addition of 1 atm H_2 to the iron dicarbyne species, affording the *Z*-olefin product $(Me_3SiO)CH=CH(OSiMe_3)$ and an unidentified paramagnetic Fe-containing product (Scheme 10, right).

Analogous to **L1Fe(μ-1,2-N₂)FeL1**, Peters and co-workers synthesized the cobalt species, **L1Co⁰(N₂)** featuring a terminal N_2 ligand and a $η^2(B,C)$ coordination of the extended σ-acceptor motif. This d^9 complex of **L1** was tested for a series of bifunctional E–H bond activations in parallel with the iron analogue, generally displaying similar reactions. Activation of benzoquinoline affords a bridging borohydride species (B–H–Co) with new Co–C and Co–N bonds (Scheme 11, left), where the heterocyclic N-atom acts as a directing group. A similar product is formed by N–H bond activation of 8-aminoquinoline. In both cases, this fifth N-donor ligand is thought to have a stabilizing effect on the formed Co^{II} species.

The reaction of **L1Co⁰(N₂)** with phenol (E = O) and thiophenol (E = S) leads to the formation of terminal Co-phenolate and Co-phenylthiolate complexes as well as 0.5 equivalent of H_2 gas (Scheme 11, right). The complexes still feature the $η^2(B,C)$ coordination mode, suggesting that the bridging borohydride species (B–H–Co) is not stable for these four-coordinated Co^{II} species. In contrast, **L1Co⁰(N₂)** activates the Si–H bond of Ph_2SiH_2 to form a bridging B–H–Co motif (Scheme 11, right). This bifunctional bond activation is similar to the observed structurally related Fe and Ni complexes [67, 74]. The formation of the B–H–Co motif is reversible and

was applied to the catalytic hydrosilylation of benzaldehydes, alkyl aldehydes and aryl and alkyl ketones, where **L1Co^0(N$_2$)** generally outcompetes the structurally related Ni system [67].

3   π-Acceptor Ligands

3.1   *Dewar-Chatt-Duncanson Model*

It is remarkable that, while Zeises' salt K[PtCl$_3$(C$_2$H$_4$)]·H$_2$O was reported in 1827 as the first organometallic complex [77, 78], it took more than 100 years to explain its olefin coordination. This complication originated from the lack of a binding model to fully interpret the observed data. The Dewar-Chatt-Duncanson (DCD) bonding model, which is widely used today to explain olefin coordination, was proposed in the 1960s by Michael J. S. Dewar, Joseph Chatt, and Leonard A. Duncanson. This model involves two important orbital interactions between the η^2(C,C)-bound olefin and the transition metal center. First, the π-electrons of the olefin double bond form a σ-bond with the transition metal (Fig. 8, left). Additionally, a filled d-orbital backdonates electron density into the π* orbital of the double bond (Fig. 8, middle).

Olefin coordination to a transition metal center can be described as two resonance extremes: the π-adduct (Fig. 8, **I**) and the metallacycle coordination (Fig. 8, **II**). Formally, the oxidation state of the metal is increased by two in the metallacycle extreme. In cases where π-backdonation is the dominating interaction, the ligand effectively accepts electron density from the transition metal making it an acceptor ligand with a low-lying π* orbital as the characteristic accessible empty orbital.

The DCD model was originally proposed for metal-bound olefin coordination but can also be applied to other π-ligands such as side-bound ketones and imines. The synthesis, coordination chemistry and metal-ligand cooperative reactivity of transition metal pincer complexes featuring these π-acceptors are discussed in the next sections.
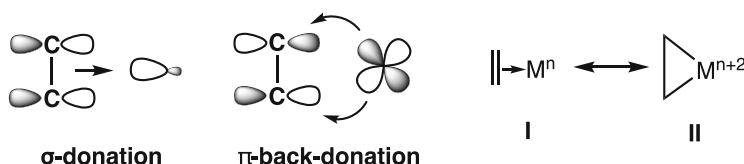

Fig. 8   Bonding description of a metal-bound olefin ligand in two orbital interactions (left) and the two resonance extremes of the DCD model (right)

3.2 Anchored Olefin-Metal Complexes: First Steps Towards Metal-Ligand Cooperativity

In general, metal-bound olefins insert readily into a M–Y bond resulting in a metal-alkyl species. Thereby the motif formally accepts either a nucleophilic or an electrophilic fragment ($Y = Nu^-$ or E^+). Such steps are often part of a catalytic cycle in which the olefin is one of the substrates and subsequently leaves the coordination sphere of the metal as a product molecule. They could potentially also be applied in the context of metal-ligand cooperative catalysis, if the reactive olefin were anchored to the metal in a pincer-type ligand design and thus forced to remain in the coordination sphere. Figure 9 (right) schematically shows the envisioned bifunctional activation of a X–Y bond across the anchored olefin-metal interaction.

In addition, the weak interaction between an olefin motif and a transition metal may be reversibly disrupted, stabilizing reactive intermediates that require different coordination environments at the metal. A pincer ligand with an olefin as central binding moiety would then act as a hemilabile ligand (Fig. 9, left). In this section, the synthesis and reactivity of pincer complexes featuring an anchored olefin motif are discussed. Here, the reversible β-hydride insertion/elimination process is central as it represents a first step towards metal-ligand cooperative reactivity using this type of π-acceptor ligands.

Rigid *o*-phenylene linkers have been abundantly used to anchor a central σ-acceptor motif in the proximity of transition metal centers (Sects. 2.2 and 2.3). Iluc and co-workers used this approach to bring a central ethyl-group into close proximity of a Pd^{II} center (Scheme 12, left) [79]. Heat-induced C–H activation and dehydrohalogenation generates a square planar PCP Pd^{II} complex (Scheme 12, middle) [80]. A second dehydrohalogenation step with potassium bis(trimethylsilyl)amide (KHMDS) leads to a Pd^0 complex featuring a metal-bound olefin motif (Scheme 12, right).
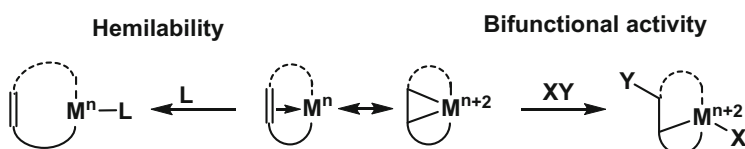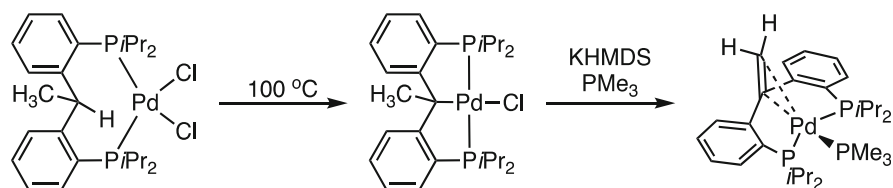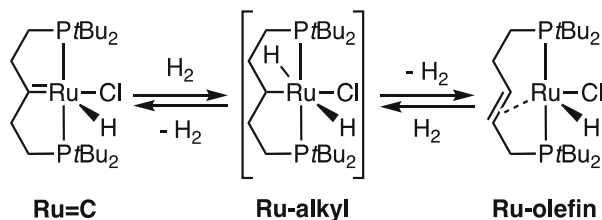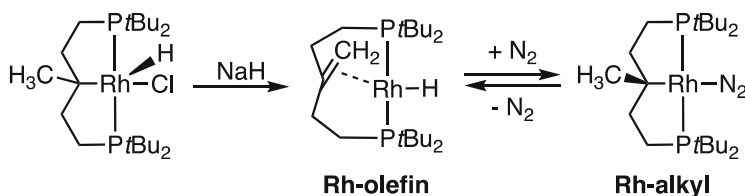

Fig. 9 Resonance extremes of a metal-bound olefin motif and their prototypical cooperative reactivity

Scheme 12 Synthesis of a metal-bound olefin motif in the coordination sphere of Pd^0 [79]

Scheme 13 The interconversion of **Ru=C** to **Ru-olefin** involves α- and β-hydride elimination and insertion processes [81]


Scheme 14 The **Rh-olefin** complex shows N_2-dependent β-hydride insertion and elimination [83]

X-ray crystallography suggests a strong interaction between Pd^0 and the bound olefin as an elongated C=C bond length of 1.398(3) Å vs 1.34 Å (for a typical C=C bond) is observed, indicating significant π-backdonation.

The Pd-olefin complex was also identified as the product of a side reaction of a Pd-bound nucleophilic carbene incorporated in a PCP pincer structure with CH_2Cl_2, in which a formal CH_2-group transfer to the nucleophilic carbon atom occurs. A perhaps less unexpected connection between a metal-bound olefin motif and a carbene complex is found in isomerization of an aliphatic PCP Ru carbene species (**Ru=C**) to a **Ru-olefin** species featuring a 1,2-connected olefin motif (Scheme 13) reported by Gusev and co-workers [81]. As postulated by Shaw and co-workers [82], the transformation is thought to go through a **Ru-alkyl** intermediate formed by initial hydrogenation and α-hydride insertion of the carbene complex. Subsequent β-hydride elimination and H_2 release form the metal-bound olefin motif. The displayed reversible transformations make systems with labile hydrogen atoms present in α- and β-position to the metal promising candidates for investigations into metal-ligand cooperative processes.

Specifically, the process of β-hydride elimination/insertion was studied by Milstein and co-workers using a metal-bound olefin motif with a 1,1-disubstitution pattern. Here, the olefin double bond reversibly inserts into a Rh–H bond (Scheme 14) [83]. An aliphatic PCP pincer complex of Rh was shown to react with sodium hydride (NaH), resulting in formal HCl elimination. Interestingly, a subsequent β-hydride elimination is observed, resulting in the formation of a metal-bound olefin motif in **Rh-olefin**. This **Rh-olefin** complex is in a fast equilibrium with the corresponding alkyl complex via olefin insertion/β-hydride elimination. Free N_2 traps the olefin insertion product by coordination to Rh to form **Rh-alkyl**. A kinetic study revealed N_2 dissociation to be the rate-limiting step in the conversion from
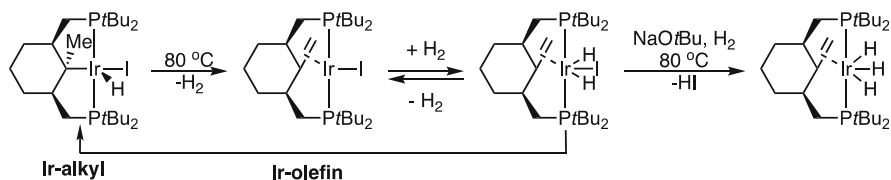
Scheme 15 Reversible H_2 activation and β-hydride insertion at the **Ir-olefin** complex [84]

Rh-alkyl to **Rh-olefin**. This equilibrium is a remarkable example of direct *trans* migration via a concerted, highly organized transition state. The insertion is thought to be possible due to the unique geometry of **Rh-olefin**, in which the square planar geometry is distorted in order to bend the olefin towards the *trans*-hydride already in the ground state. Overall, this system demonstrates that facile and reversible β-hydride elimination/insertion is possible even with the natural *trans* configuration imposed by the pincer structure and shows the potential of π-complexes to act as a transient hydride storage moiety in cooperative processes.

In a related study by Wendt and co-workers, **Ir-olefin** (Scheme 15) was synthesized starting from **Ir-alkyl**, an aliphatic PCP pincer complex featuring a methyl-substituted cyclohexyl ring [84]. In the reaction, dehydrogenation was induced upon heating, leading to the formation of a metal-bound olefin motif. In this process, the C–C bond length decreases from 1.553(4) Å in **Ir-alkyl** to 1.438(15) Å in **Ir-olefin**. This distance being between the typical ranges for C–C single and double bonds indicates strong π-backdonation from the electron-rich Ir center to the olefin motif.

In the presence of H_2, **Ir-olefin** is in equilibrium with the corresponding Ir^{III}-dihydride complex. Furthermore, upon heating, a stable Ir^{III}-trihydride complex (Scheme 15, right) can be obtained by formal hydrogen iodide (HI) elimination with NaOtBu in the presence of a H_2 atmosphere. The Ir^{III}-trihydride species does not release a H_2 molecule or undergo β-insertion. In contrast, a hydride in the Ir^{III}-dihydride complex slowly inserts into the olefin double bond, reinstating the initial **Ir-alkyl** complex. The shuffling between metal-olefin and metal-alkyl species by means of a reversible β-hydride insertion/elimination process enables the cooperative activation of small molecules as was presented by Wendt and co-workers. They used the slightly different Ir complex (**Ir-Ph**, Scheme 16) featuring a coordinated, internal C=C bond [85]. A comparably strong metal-olefin interaction is indicated by the C=C bond elongation to 1.425(7) Å according to X-ray crystal structure determination. **Ir-Ph** readily activates H_2 to form the corresponding Ir^{III}-trihydride complex (**Ir-(H)₃**). A subsequent, reversible H_2 addition coupled to β-insertion generates an equilibrium between the two Ir species **Ir-(H)₃** and its corresponding insertion product **Ir-(H)₄**. The latter features a central C_{sp3} donor atom and is characterized as a tetrahydride by NMR spectroscopy. In addition, the described β-hydride insertion/elimination process is observed in the reversible CO_2 addition to **Ir-(H)₃** (Scheme 16, bottom). This reactivity constitutes an interesting example of metal-ligand cooperativity where insertion of CO_2 into the Ir–H bond is coupled to a β-hydride insertion to form the Ir^{III}-formate species (**Ir-OC(O)H**) [86].
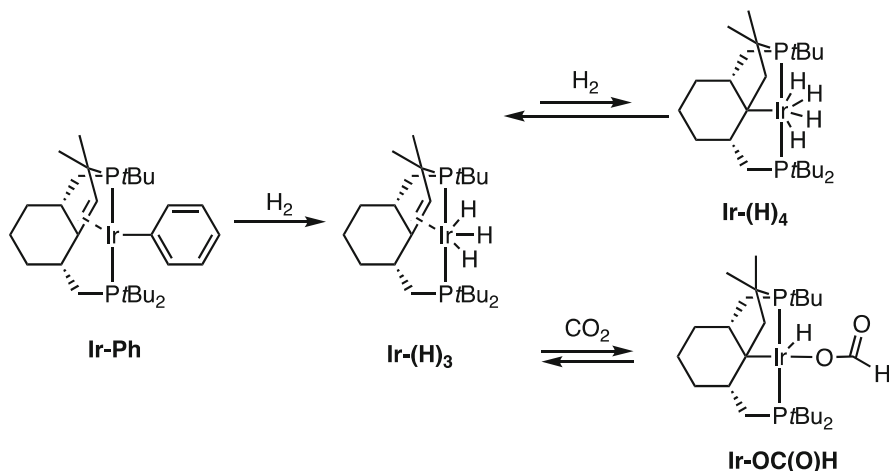
Scheme 16 Metal-ligand cooperative reactivity of **Ir-(H)₃** with H_2 and CO_2 [85, 86]
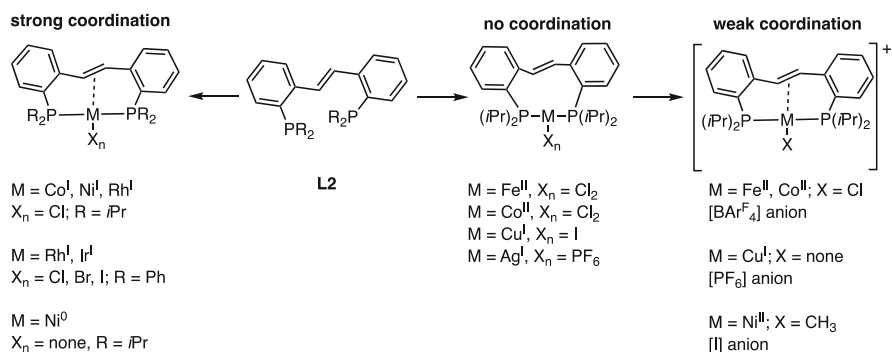
Scheme 17 Overview of the different coordinative interactions between a transition metal center and **L2** [87–89]

The discussed examples show that a π-acceptor olefin ligand in the central position of a pincer ligand can reversibly accept a hydride ligand from the metal it is bound to, opening up possibilities for bifunctional substrate activation as depicted in Fig. 9 (right). The utility of an olefin as a hemilabile moiety (Fig. 9, left) is more apparent in the chemistry of a related ligand family in which the central olefin is connected to the phenylene linkers in a 1,2 fashion instead of the 1,1-connectivity discussed so far. A systematic analysis of the coordination of such ligands to different transition metal centers in different oxidation states was conducted by Iluc and co-workers. The used olefin ligand (**L2**, Scheme 17) is designed to bind in a κ³(P,C=C,P) fashion with an η² coordination of the olefin. Indeed, the pincerlike coordination of **L2** is observed for electron-rich transition metals of groups 8, 9, and 10, while no coordination of the central olefin motif is observed for more electron-poor transition metal centers such as Fe^II and Co^II (Scheme 17) [87–91]. In addition,
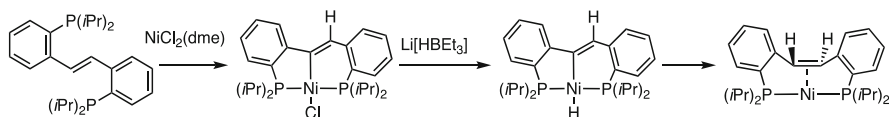
Scheme 18 Synthesis of a vinyl-Ni^{II} complex formation from **L2** and a Ni^{II} source and reduction of the vinyl-Ni^{II} complex with a hydride source to form the electron-rich Ni^0 center [88]
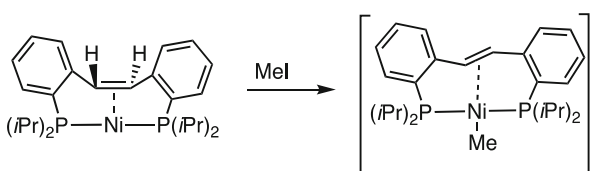

Scheme 19 Reaction of **L2Ni^0** with MeI to form a cationic methyl Ni^{II} complex [88]

halide abstraction at **L2Fe^{II}Cl$_2$** and **L2Co^{II}Cl$_2$** with NaB(Ar^F)$_4$ leads to a weak olefin coordination (Scheme 17, right) best described as a π-adduct with weak π-backdonation. Integration of an olefin in a chelating ligand such as **L2** enables a flexibility in coordination strength of the central motif that is usually not associated with pincer ligands.

The distinction between weak and strong olefin coordination is based on M–C bond distances and C=C bond elongation. For instance, the C=C bond length in free **L2** is 1.330(4) Å, weak η^2 (C,C) coordination of the motif in **[L2Co^{II}Cl][B(Ar^F)$_4$]** leads to an elongation of the bond to 1.397(6) Å, and strong coordination as in **L2Co^{I}Cl** elongates the C=C bond even more to 1.442(5) Å. Therefore, **L2** functions as an adaptive π-acceptor ligand since it stabilizes transition metal centers in different oxidation states by means of withdrawing electron density to various extents.

Upon coordination of **L2** to NiCl$_2$(dme), formal proton abstraction from the C=C bond and overall HCl elimination yields a vinyl-Ni^{II} complex (Scheme 18) [88]. The formation of similar vinyl pincer complexes is also observed upon coordination of **L2** to precursors of Pd^{II} and Pt^{II} [89]. The vinyl-Ni^{II} complex can react with a hydride source (Li[HBEt$_3$]) to initially form a vinyl-Ni-H species. Over time, reductive elimination of the C–H bond leads to the formation of **L2Ni^0** featuring the metal-bound olefin motif. **L2Ni^0** can be synthesized directly in a reaction of Ni(COD)$_2$ with **L2** [88]. This Ni^0 complex adopts a pseudotrigonal-planar geometry in which the *trans* olefin motif is twisted out of the P–Ni–P plane. An elongated C=C bond distance of 1.406(5) Å indicates significant π-backdonation from the electron-rich Ni^0 center to the olefin motif. More importantly, this shows that **L2** gives access to electron-rich transition metal centers of low oxidation state.

η^2 coordination of the olefin motif is also observed in Ni species of higher oxidation state. In a reaction of **L2Ni^0** with methyl iodine (MeI), a cationic methyl nickel complex (**[L2Ni^{II}Me]I**, Scheme 19) is formed. An elongation of the C–C bond distance to 1.383(3) Å indicates weaker π-backdonation in this Ni^{II} cation than in **L2Ni^0**.
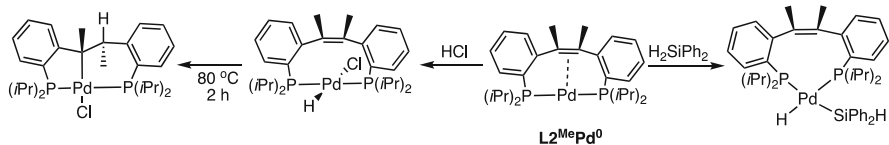
Scheme 20 Protonation of $L2^{Me}Pd^0$ with HCl affords a vinyl Pd species (left) and synthesis of a Pd^{II} species by oxidative addition of H_2SiPh_2 to $L2^{Me}Pd^0$ (right) [92]
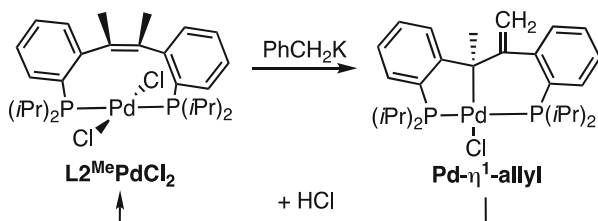
**Scheme 21** Reversible deprotonation of one methyl group in $L2^{Me}PdCl_2$ [92]

L2 coordination to $(dba)_2Pd$ results in a dimeric product [88]. However, an analogue **L2** possessing two methyl substituents on a central Z-olefin ($L2^{Me}$) affords a monomeric $L2^{Me}Pd^0$ product (Scheme 20) for which η^2 coordination of the olefin motif was verified by X-ray diffraction crystallography [92]. Oxidative addition of the Si–H bond in H_2SiPh_2 to $L2^{Me}Pd^0$ results in the formation of a distorted square planar Pd^{II} species in which the olefin motif has decoordinated (Scheme 20, right). Hence, $L2^{Me}$ acts as a hemilabile ligand, adapting to the electronic requirements of the Pd center in both oxidation states.

In a reaction of $L2^{Me}Pd^0$ with HCl, initial oxidative addition to form the Pd^{II} species is observed similar to the reaction with H_2SiPh_2. However, upon heating the sample for 2 h at 80°C, a vinyl Pd^{II} pincer complex is obtained most likely by β-hydride insertion (Scheme 20, left). Though attempts to deprotonate the vinyl Pd species with a base failed, the transformation in Scheme 20 suggests a promising hydrogen acceptor capability of the π-acceptor olefin motif in $L2^{Me}Pd^0$. Similar to this, early work by Bennet and co-workers showed the synthesis of a vinyl Rh complex by formal protonation of the olefin backbone in $L2Rh^I(CO)Cl$ with HCl leading to the formation of a new M–C σ bond [93].

Dehydrohalogenation of the Pd^{II} complex $L2^{Me}PdCl_2$ was observed in a reaction with benzyl potassium ($PhCH_2K$). The η^1-allyl Pd^{II} product (**Pd-η^1-allyl**, Scheme 21) contains a terminal olefin motif which was formed by deprotonation of one methyl group as evident from a new set of doublet of doublet signals at 4.85 ppm and 4.63 ppm in ^1H NMR. In addition, an X-ray crystal structure of this asymmetric species confirms the double bond character of the new motif (C–C bond distance, 1.366(5) Å; Fig. 10). Facile protonation of **Pd-η^1-allyl** with HCl cleanly forms $L2^{Me}PdCl_2$ again, showing the deprotonation to be reversible.

Overall, a variety of stoichiometric processes involving metal-ligand cooperativity at the central olefin position of pincer ligands have been discussed. Specifically, these include several examples of facile and reversible β-hydride

Fig. 10 X-ray crystal structure of **Pd-η¹-allyl** showing the new C2=C4 double bond motif (thermal ellipsoids at 50% probability). Hydrogen atoms and iPr-groups on the phosphorus atoms (except for the olefin-bound carbon atoms) are omitted for clarity [92]
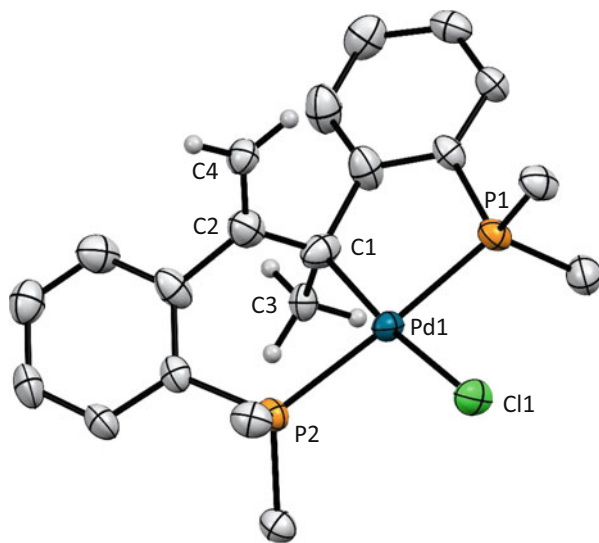
elimination/migratory insertion in which the olefin transiently stores a hydride equivalent. In addition, metal-centered reactivity can be facilitated by (de)-coordination of the olefin moiety. Such processes have the potential to become part of catalytic cycles in further investigations. In the next section, the role of a π-acceptor ketone motif in metal-ligand cooperative catalysis is highlighted.

3.3 Metal-Ligand Cooperative Catalysis Induced by Side-On Coordination of a Ketone

Due to the electronegativity of oxygen, both the π(C, O) and the π*(C, O) orbital of a ketone are lower in energy than those of an olefin. This can be anticipated to render side-on bound ketones both weaker donors and stronger acceptors than olefins. In addition, the lone pairs on the oxygen atom in the ketone motif offer an additional position for reactivity and metal-ligand cooperativity. However, free ketones preferentially coordinate end-on η^1(O) to most transition metal centers, while side-on η^2(C,O) coordination is required for a ketone motif to act as a π-acceptor ligand (Fig. 11).

Incorporation of the ketone motif into a rigid pincer design featuring *o*-phenylene linkers brings the motif into close proximity of the transition metal center in a pre-oriented geometry favoring side-on binding. The phosphine-tethered ketone ligand **L3** (Fig. 11, box) was first reported by Ding and co-workers, who used its Ru complexes in the catalytic hydrogenation of ketones [94]. While itself achiral, **L3** was proposed to enhance enantioselectivity by mechanically transferring chiral information from a chiral diamine ligand onto the Ru-bound substrate. In addition,
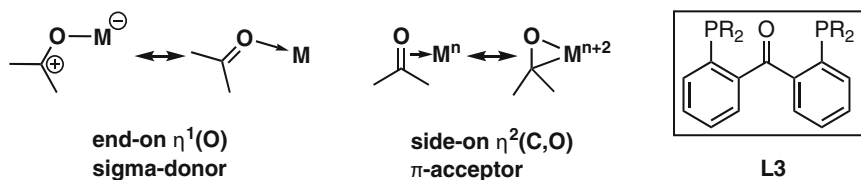
Fig. 11 End-on η^1(O) and side-on η^2 (C,O) coordination modes of ketones to transition metal center; the phosphine-tethered ketone ligands **L3** (box)
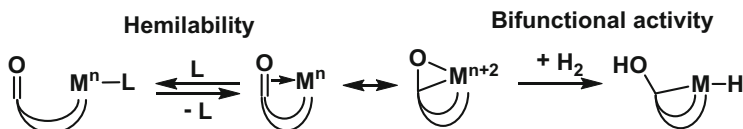

Fig. 12 Resonance extremes of a η^2 (C,O)-coordinated ketone motif and their prototypical cooperative reactivity
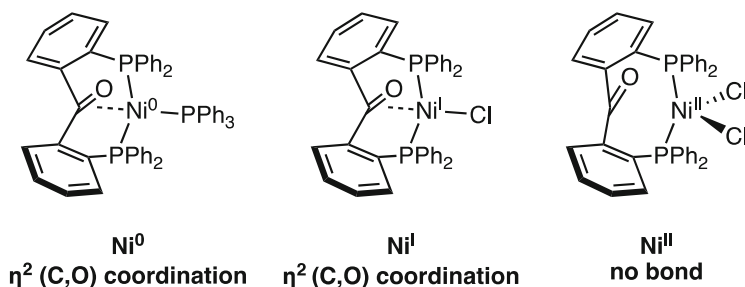
Fig. 13 The phosphine-tethered ketone ligand **L2** and its coordination chemistry to Ni^0, Ni^I, and Ni^{II} [95]

side-on coordination of the ketone motif was determined by X-ray crystallography, and this carbonyl coordination to the catalytically active Ru^{II} species was suggested to be essential for high yields and selectivity.

In the following, the coordination chemistry of **L3** to late transition metal centers and metal-ligand cooperative catalysis using these **L3**-TM complexes is presented. First, the hemilabile coordination behavior (Fig. 12, left) of **L3** is discussed, as well as its implications for catalysis. Second, the ability of the ketone motif to act a hydride relay is examined in the context of bifunctional H$_2$ activation (Fig. 12, right).

Moret and co-workers studied the coordination of **L3** to a redox series of Ni (Ni^0, Ni^I, and Ni^{II}) [95]. The ligand binds in a κ^3(P,C=O,P) fashion with η^2(C,O) coordination of the ketone motif to the electron-rich Ni^0 and Ni^I centers but adopts a κ^2(P,P) mode with the electron-poor, high-spin Ni^{II} center, thereby adapting its coordination mode to the electronic structure of nickel (Fig. 13). In addition, NBO analysis on optimized geometries of all three Ni species indicated significant charge

Fig. 14 Resonance structures of M^I ketone complexes [96]
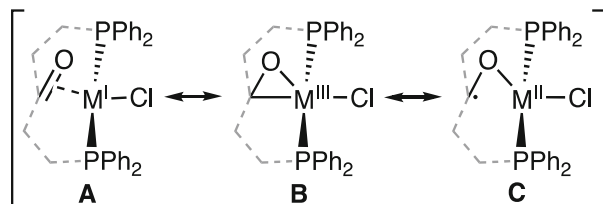
transfer from the Ni center to the ketone, supporting its description as an acceptor moiety.

This coordination behavior of **L3** is rather general for late first-row transition metal centers. The ketone motif does not coordinate to electron-poor Fe^{II}, Co^{II}, and Ni^{II} [96], but side-on coordination is detected in electron-rich transition metal complexes of **L3** (Ni^0 [95], Ni^I, Fe^I, Co^I [97], Pd^0 [98], Rh^I [99], and Ru^{II} [94]). Interestingly, in isostructural Ni^I, Co^I, and Fe^I complexes of **L3**, an increase in the amount of charge transfer upon binding (longer C–O distance) correlates with a longer M–C and a shorter M–O bond distance [96]. The opposite would be expected from the increase of π-backdonation into the primarily carbon-centered π* orbital. This apparent discrepancy was rationalized by proposing a (minor) contribution of a third resonance structure involving a ketyl radical interacting with M^{II} in addition to the resonance extremes of the DCD model (Fig. 14). Though small, the increasing contribution of this ketyl resonance structure in the trend from Ni^I to Fe^I would account for a stronger ionic M–O bond and a weaker M–C bond while maintaining an increasing electron donation to the motif.

The consequences of the observed hemilability of **L3** were investigated using the Ni-catalyzed alkyne cyclotrimerization reaction as a benchmark reaction. Under optimized conditions, the Ni complex **L3Ni^0(BPI)** (BPI = benzophenone imine, a labile co-ligand) converts terminal alkynes selectively into the corresponding 1,2,4-substituted trimerization products (Table 3, entry 1) [100]. The catalysis was tested for six substrates (R = Ph, CO_2Me, CH_2OMe, CO_2Et, 4-F-C_6H_4, 4-OMe-C_6H_4) showing a higher yield for an electron-withdrawing substrate. In all investigated cases, at most very small amounts of cyclooctatetraene (COT) by-products are formed.

The activity of **L3Ni^0(BPI)** was compared to the performance of Ni complexes featuring a pincer-type trisphosphine (PPP) or a bidentate diphosphine ether (POP) supporting ligand (Table 3, entries 2 and 3). **L3Ni^0(BPI)** outcompetes these systems in catalytic activity and selectivity indicating an advantage of a π-acceptor motif for this reaction. To further rationalize the role of the ketone moiety, a mechanistic study relying on experimental and computational data was conducted, and a catalytic cycle was proposed, which is shown in Fig. 15. For the computational work, acetylene was used as a model substrate (R = H), and phenyl substituents replaced the *p*-tolyl substituents on the P-donor moieties.

In the stable, 18 VE **L3Ni^0(BPI)** precatalyst, the ketone moiety masks a coordination site by η^2(C,O) coordination as evident from a characteristic chemical shift of the carbonyl triplet signal at 119.0 ppm in ^{13}C NMR. A downfield shift of this

Table 3 Comparative study of the Ni-catalyzed alkyne cyclotrimerization reaction (P^4 = P (p-tolyl)$_2$, P^1 = PPh$_2$) [100]

| terminal alkyne | | 1,2,4-trimer | 1,3,5-trimer | tetramers (COTs) |

Ni-catalyst	R =	Yield 1,2,4-trimer (a)	Yield 1,3,5-trimer (b)	Yield COTs (c)	Ratio a/b/c
1)	Ph	86.9	3.2	0	97:3:0
	CO$_2$Me	90.2	6.3	2.5	91:7:2
2)	Ph	3.1	1.9	0	62:38:0
	CO$_2$Me	24.5	2.1	7.5	72:6:22
3)	Ph	2.8	0.2	0	94:6:0
	CO$_2$Me	65.0	12.3	6.5	77:15:8

carbonyl ^{13}C NMR signal to 202.7 ppm indicates that the occupied site is readily freed up to allow alkyne binding (step 1). This ligand exchange results in a Ni^0 alkyne complex, which is also the in situ observed resting state of the catalyst. Geometry optimization of the bis(acetylene) Ni complex indicates that the ketone moiety remains decoordinated during the second alkyne uptake (step 2). Remarkably, the oxidative coupling step (step 3) is facilitated by concomitant ketone η^2(C,O) coordination, which stabilizes the resulting Ni^{II} metallacyclopentadiene intermediate. In the calculated trigonal-bipyramidal structure, the two P-atoms occupy the axial positions, and elongation of the C–O bond indicates a strong interaction of the Ni^{II} center with the η^2(C,O)-coordinated ketone motif. This is presumably a result of strong σ-donation by the C-atoms of the metallacyclopentadiene into the d-orbital that backdonates into the π*(C,O) orbital, which is parallel to the equatorial plane. As the oxidative coupling step is widely acknowledged to be the rate-determining step of the strongly exothermic
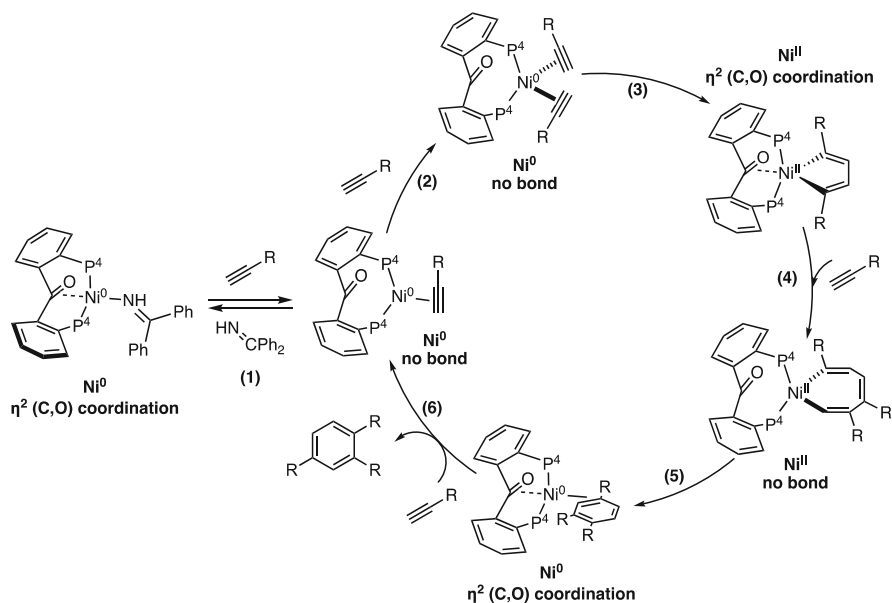
Fig. 15 Proposed catalytic cycle for the **L3Ni⁰(BPI)** catalyzed cyclotrimerization of terminal alkynes, $P^4 = P(p\text{-tolyl})_2$ [100, 101]

cyclotrimerization reaction, stabilization of the intermediate directly following the rate-determining step accelerates the overall reaction. Consecutive alkyne coordination and migratory insertion processes lead to the formation of a nickelacycloheptatriene intermediate (step 4) in which the carbonyl has decoordinated to accommodate alkyne coordination [101]. Finally, reductive elimination to obtain the trimerization product (step 5) and ligand exchange with an incoming alkyne substrate (step 6) close the catalytic cycle. Interestingly, the Ni-trimer adduct formation (step 5) is thought to be accelerated by facile ketone coordination as evident from a small activation free energy ($\Delta G^{o,\ddagger} = +0.8$ kcal/mol) [101]. The saturated Ni^{II} complex is less likely to insert a fourth equivalent of alkyne to form COTs, which accounts for the increased selectivity of **L3Ni⁰(BPI)** for cyclotrimerization products. Overall, the adaptive coordination behavior of the π-acceptor ketone ligand along the reaction coordinate of the alkyne cyclotrimerization reaction explains the enhanced catalytic activity and selectivity of **L3Ni⁰(BPI)**, making this approach promising for future catalyst development.

A pincer ligand featuring a π-binding central unit can also be synthesized in the coordination sphere of a transition metal. In this vein, Iluc and co-workers demonstrated the synthesis of a η^2(C,E)-coordinated chalcogen ketones ($R_2C = E$, E = S, Se, Te) in the coordination sphere of a Pd^{II} pincer featuring a nucleophilic carbene at the central position (Scheme 22) [98]. The Pd-carbene compound reacted with elemental sulfur, selenium, or tellurium to form new C = E bonds. In contrast, the
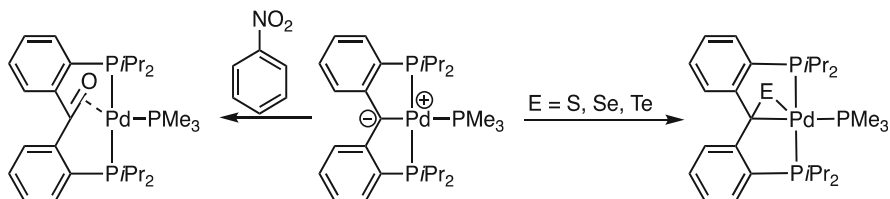
Scheme 22 Conversion of a nucleophilic Pd^{II} carbene complex to various η^2(C,E)-coordinated chalcogenoketone Pd complexes by formal O, S, Se, and Te atom transfer [98]
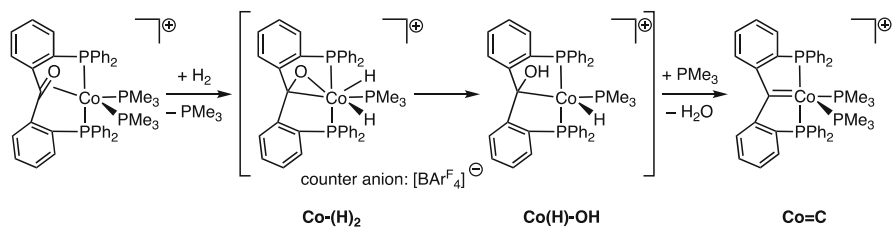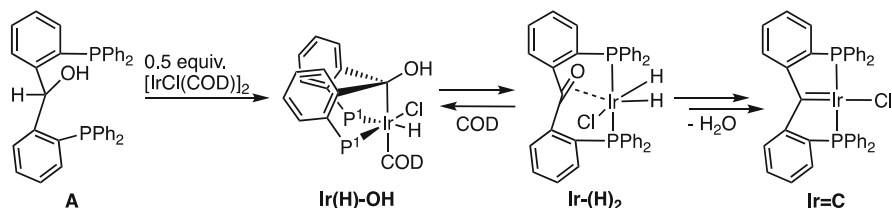

Scheme 23 Synthesis of the Co carbene pincer **Co=C** by reductive deoxygenation proposed to occur via a metal-ligand cooperative process [97]

complex did not react with O_2; instead, half of an equivalent of nitrobenzene quantitatively yielded the ketone complex (Scheme 22, left).

Based on X-ray crystallography, the extent of C = E multiple bonding in the complex decreases from oxygen to tellurium. Significant double bond character is observed for E = O, S, only residual π-bonding is found for E = Se, and the C–Te bond length is typical for a sp^3-C–Te single bond. The ^{13}C NMR data shows a similar trend, where the coordinated C=O bond gives rise to the most downfield resonance (160.4 ppm) and the others shift upfield following the decreasing electronegativity of the chalcogens (S: 114.6 ppm; Se: 112.5 ppm; Te: 102.4 ppm). Further reactivity studies of these new π-ligands incorporating heavier chalcogens would certainly be of interest.

The abovementioned conversion of a carbene species into a η^2(C,O)-coordinated ketone by formal oxygen atom transfer can also be reversed. The group of Young investigated the reductive deoxygenation of group 9 ketone complexes to form the corresponding carbene species. The five-coordinate, cationic **[L3Co^I(PMe$_3$)$_2$] [BAr$^F_4$]** complex featuring a η^2(C,O)-coordinated ketone moiety was synthesized by coordination of **L3** to [Co(PMe$_3$)$_4$][BAr$^F_4$]. In the presence of H_2 gas, reductive deoxygenation of **[L3Co^I(PMe$_3$)$_2$][BAr$^F_4$]** to form the PCP Co carbene species **Co=C** is observed (Scheme 23) [97]. The proposed reaction pathway involves homolytic H_2 activation to form the dihydride species **Co-(H)$_2$**, a subsequent insertion of the ketone double bond into one Co–H bond to yield the hydroxylalkyl cobalt-hydride intermediate **Co(H)-OH** and H_2O elimination to obtain the final carbene product **Co=C**. The two intermediates, **Co-(H)$_2$** and **Co(H)-OH**, are

Scheme 24 Synthesis of the iridium carbene pincer **Ir=C** by initial coordination of **A** to the Ir precursor ([IrCl(COD)]$_2$) and subsequent cooperative H$_2$O elimination, P^I = PPh$_2$ [102]
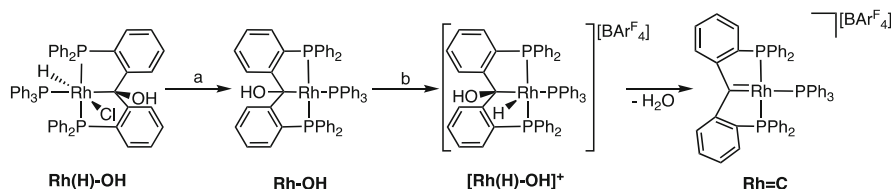
Scheme 25 Synthesis of Rh=C from an α-hydroxylalkyl Rh^I complex (**Rh(H)-OH**) by reaction with (**a**) LiHMDS and (**b**) [H(OEt$_2$)$_2$][BAr$^F_4$] [99, 103]

proposed for this transformation based on mechanistic studies performed on the corresponding Ir-[102] and Rh-systems [99, 103].

First, the synthesis of the PCP Ir carbene species **Ir=C** by dehydration of the alcohol ligand (**A**, Scheme 24) is considered [102]. Here, in the reaction of **A** with 0.5 equivalent of [IrCl(COD)]$_2$, an α-hydroxylalkyl Ir^{III} complex (**Ir(H)-OH**) was characterized by in situ low-temperature NMR spectroscopy. The complex is in equilibrium with a η^2(C,O) keto Ir dihydride species (**Ir-(H)$_2$**) as evident from a ^{13}C NMR signal at 132.1 ppm. This indicates that a β-hydride insertion/elimination process reversibly converts **Ir-(H)$_2$** into **Ir(H)-OH** in which the ketone motif in **Ir-(H)$_2$** can be seen as a hydride relay. **Ir-(H)$_2$** was also observed in situ in the reaction of **L3**, [IrCl(COD)]$_2$ and H$_2$. Though the subsequent H$_2$O elimination to form **Ir=C** is not a clean reaction as the carbene species is further reduced by excess H$_2$ gas, the second synthesis route of **Ir-(H)$_2$** establishes a connection between **L3** and **Ir=C**.

The stepwise synthesis of the PCP Rh carbene species **Rh=C** proceeds via an isolable α-hydroxylalkyl Rh^{III} hydride species (**Rh(H)-OH**; Scheme 25) [99]. **Rh (H)-OH** is synthesized by reaction of **A** with [RhCl(COD)(PPh$_3$)]. The X-ray structure shows that upon C–H activation, the ligand adopts a *mer* configuration (Fig. 16). Interestingly, the hydroxyl hydrogen forms a hydrogen bridge to the chloride co-ligand, suggesting a relatively high acidity of this proton. Indeed, the ^{1}H NMR signal for the hydroxyl proton, located at 7.57 ppm, disappears upon the addition of D$_2$O. Moreover, HCl elimination to form an α-hydroxylalkyl Rh^I complex (**Rh-OH**) is observed upon treatment of **Rh(H)-OH** with LiHMDS.

Rh-OH can also be synthesized from **L3** and the [RhH(PPh$_3$)$_4$] precursor. Upon protonation of **Rh-OH** with Brookhart's acid, **Rh=C** is immediately formed by H$_2$O elimination [103]. Most likely, the cationic Rh species [**Rh(H)-OH**]$^+$ is an
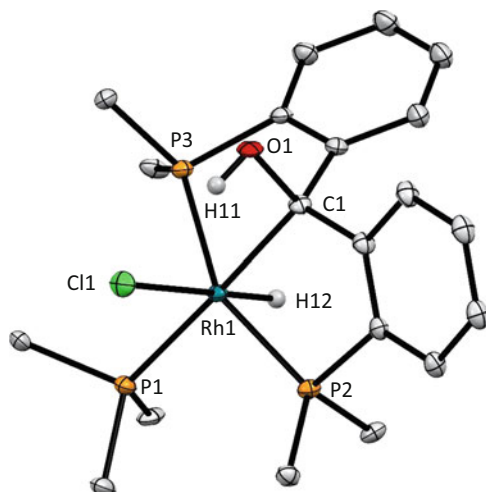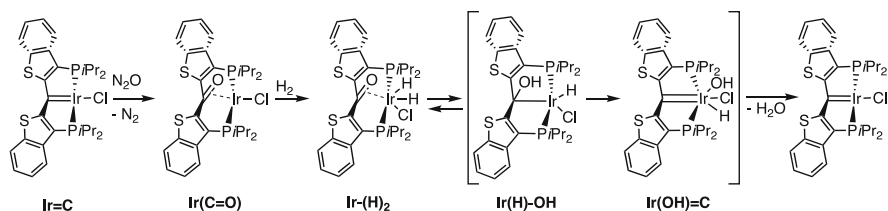
Fig. 16 X-ray crystal structure of **Rh(H)-OH** showing the α-hydroxylalkyl group (thermal ellipsoids at 50% probability). Hydrogen atoms (except H11 and H12) and phenyl groups on the phosphorus atoms (except for the bound carbon atom) are omitted for clarity [99]

Scheme 26 Cooperative deoxygenation of N_2O by **Ir = C** to form the η^2 (C,O)-coordinated ketone Ir complex. Subsequent cooperative deoxygenation involves H_2 activation, β-hydride insertion, α-hydroxyl group migration, and H_2O elimination to reestablish **Ir=C** [104–106]

intermediate in this reaction. More generally, α-hydroxylalkyl metal-hydride species are proposed as intermediate in the reductive deoxygenation of **L3** to form the corresponding carbene species.

A possible mechanism for H_2O elimination as last step in the overall reductive deoxygenation reaction has been suggested by Piers and co-workers. For this study, a related Ir carbene pincer compound affords a stoichiometric cycle for the deoxygenation of N_2O with H_2 [104]. Scheme 26 shows the different transformations starting from a reaction of the Ir carbene complex (**Ir=C**) with N_2O to form the η^2(C, O) ketone complex (**Ir(C=O)**). Subsequent reduction with H_2 results in the elimination of the oxygen atom in the form of H_2O.

The reaction of **Ir(C=O)** with H_2 affords the adduct **Ir-(H)$_2$** that exists as a *cis* isomer (depicted in Scheme 26) and a *trans* isomer (not depicted), the former being the kinetic product and the latter the thermodynamic product of the reaction. When a H_2/D_2 gas mixture is used, H/D scrambling to obtain **Ir-(H)$_2$**, **Ir-(D)$_2$**, **Ir-(HD)**, and
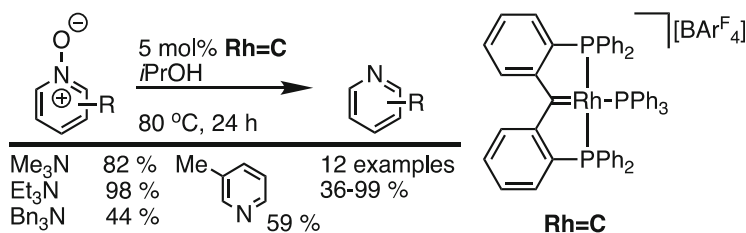
Fig. 17 Catalytic deoxygenation of amine- and pyridine N-oxides [107]

Ir-(DH) is mediated by the kinetic *cis* isomer [105], which was proposed to proceed via a reversible β-hydride insertion into the ketone bond followed by activation of a second hydrogen molecule by the resulting hydroxylalkyl/hydride compound **Ir(H)-OH**. At high temperatures, the α-hydroxyl group in **Ir(H)-OH** is thought to migrate to the Ir center forming **Ir(OH)=C** [105, 106]. A high-energy barrier is expected for this step, which offers an explanation for the high reaction temperature ($>100°C$) required for the H_2O elimination process. The subsequent reductive elimination of H_2O from **Ir(OH)=C** occurs rapidly.

The cooperative manner in which the ketone motif operates in these examples of oxygenation and (reductive) deoxygenation demonstrates how π-acceptors can diversify the reactivity pathways of a transition metal complex. The stoichiometric examples have inspired the use of **Rh=C** as catalyst in the deoxygenation of amine and pyridine *N*-oxides to form amines and pyridines (Fig. 17) [107]. Isopropanol (*i*PrOH) proved to be a good hydrogen source compared to H_2 or $SiHEt_3$ since it prevents overreduction. Under optimized conditions, a range of amine and pyridine *N*-oxides were converted into the corresponding amines and pyridines with moderate to excellent yields. Alkyl- and arylamine *N*-oxides are generally converted in high yields to their desired products. In addition, high yields of quinoline and substituted pyridine products are obtained with a tolerance for electron-withdrawing and electron-donating substituents.

Based on stoichiometric reactions, a mechanism for the catalytic transformation of amine *N*-oxide to amine was proposed (Fig. 18). In the first step, the **Rh=C** deoxygenates the trimethylamine *N*-oxide ($ONEt_3$) substrate to form the triethylamine (Et_3N) product as well as the Rh-ketone species (**Rh(C=O)**). In a second step, **Rh(C=O)** is reductively deoxygenated by a reaction with *i*PrOH to close the catalytic cycle. Under the same catalytic conditions, **Rh(C=O)** was also used as catalyst for the deoxygenation of $ONEt_3$, yielding 62% of NEt_3 (vs 98% for **Rh=C**). The lower productivity can be ascribed to the required deoxygenation of **Rh (C=O)** to **Rh=C** prior to the first catalytic turn over.

Overall, formal oxygen atom transfer reactions interconverting a transition metal-carbene complex and a $\eta^2(C,O)$ bound ketone complex were employed in stoichiometric and catalytic deoxygenation reactions. These examples establish a proof of concept involving a side-on coordinated ketone motif as hydride relay. The discovery of this novel metal-ligand cooperative mode is promising for future development of homogeneous catalysts.
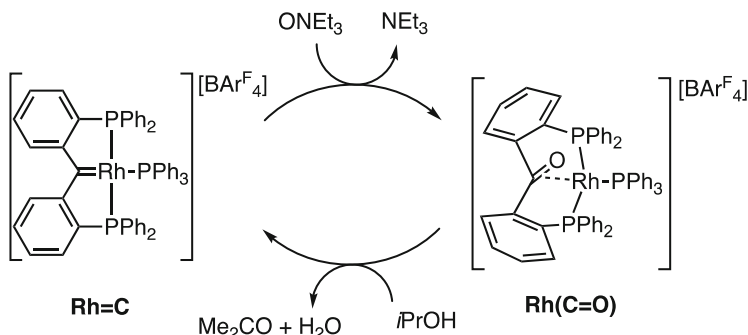
Fig. 18 Proposed catalytic cycle for the deoxygenation of amine and pyridine N-oxides [107]
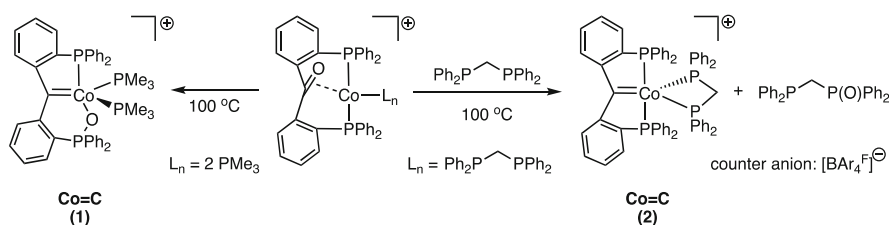
Scheme 27 Synthesis of **Co=C** species by direct oxygen atom transfer [108]

Recently, Young and co-workers reported on the synthesis of Co carbene species by direct oxygen atom transfer (Scheme 27) [108]. Two Co ketone complexes were synthesized incorporating either one bidentate dppm (1,1-bis(diphenylphosphino)-methane) or two monodentate PMe_3 co-ligands. Upon heating the **[L3Co^I(PMe$_3$)$_2$] [BAr$^F_4$]** complex, a carbene motif is formed in the product **Co=C (1)** as the oxygen atom migrates to one of the pincer flanking phosphine groups. The mechanism of this oxide transfer was investigated by DFT, where, surprisingly, the first step involves one pincer flanking phosphine group decoordinating from the Co center. The subsequent oxygen atom transfer step is exergonic and proceeds through a single transition state featuring relative short Co–C and P–O bond distances, indicating concomitant formation of the M=C and P–O bonds. It was additionally hypothesized that a bidentate phosphine co-ligand could function as a sacrificial oxygen acceptor via hemilabile dissociation. Indeed, in the presence of a second equivalent of dppm, the desired **Co=C (2)** species is obtained from **[L3Co^I(dppm)] [BAr$^F_4$]** by direct oxygen atom transfer to dppm.

3.4 Imine Side-On Coordination: Synthesis and Metal-Ligand Cooperative Reactivity

Imines can also act as π-acceptor ligands when coordinating side-on to a transition metal center. As for ketones, the $\pi(C, N)$ and the $\pi^*(C, N)$ orbitals of an imine are generally lower in energy compared to olefins, making a side-bound imine motif a stronger π-acceptor and a weaker donor ligand. Furthermore, the lone pair on the nitrogen atom in the imine motif represents an extra position for additional reactivity and metal-ligand cooperativity. While there is an abundance of examples showing $\eta^1(N)$ coordination of imines to transition metal (Fig. 19, left), $\eta^2(C,N)$ side-on coordination of imines (Fig. 19, right) to a transition metal is less frequently observed.

Incorporation of the imine motif into a rigid pincer ligand design can be used to encourage $\eta^2(C,N)$ coordination, enabling the study of imine motifs as π-acceptor ligands. The phosphine-tethered imine ligand (**L4**, [109] Scheme 28) can access two distinct binding modes. A $\eta^1(N)$-coordination of **L4** to electron-poor transition metal centers such as Co^{II} [110, 111], Ni^{II} [110, 112], and Pd^{II} [111, 112] is observed (Scheme 28, left), while a side-on $\eta^2(C,N)$ coordination to Ni^0 is preferred (Scheme 28, right). X-ray diffraction analysis of the **L4Ni⁰(PPh₃)** species shows an elongated C–N bond suggesting substantial metallacycle character of the M–C–N interaction. In ^{13}C NMR spectra, the characteristic signal of the imine carbon shifts significantly from 160 ppm in free **L4** to 84 ppm in **L4Ni⁰(PPh₃),** indicating the rehybridization of the imine motif from sp^2 to sp^3.

Metal-ligand cooperative processes employing π-acceptor imine ligands are fairly unexplored and **L4** has attractive properties for such investigations. For instance, **L4** is suited to electronically stabilize electron-rich transition metal centers of low oxidation states by coordinating $\eta^2(C,N)$ to the metal center. Moreover, **L4** coordinates as an adaptive ligand, changing its hapticity according to the electronic properties of the metal center (Fig. 20, left). In addition, bifunctional substrate

end-on η¹(N)
sigma-donor

side-on η²(C,N)
π-acceptor
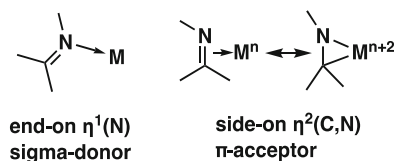
Fig. 19 End-on $\eta^1(N)$ and side-on η^2 (C,N) coordination modes of an imine to a transition metal center

σ-complex

π-complex

η¹ (N) coordination

L4
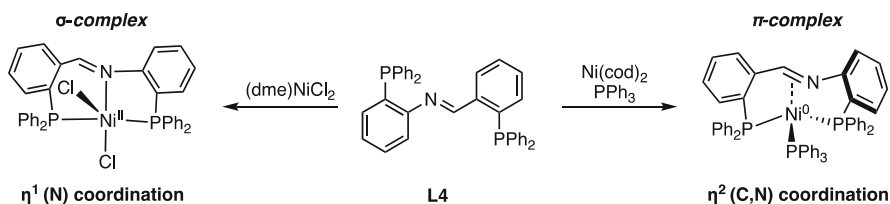
η² (C,N) coordination

Scheme 28 **L4** coordinates end-on $\eta^1(N)$ to Ni^{II} and side-on η^2 (C,N) to Ni^0 [113]

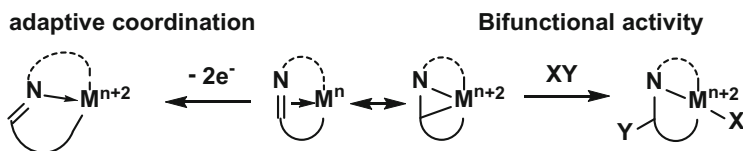**adaptive coordination**   **Bifunctional activity**

Fig. 20 Resonance extremes of a η^2 (C,N)-coordinated imine and their prototypical cooperative reactivity

activation at the metal-imine interaction could be imagined, where the imine double bond inserts into a M–Y bond (Fig. 20, right).

Upon coordination of **L4** to Ni^0 in the presence of 1 atm CO gas, the oxidative coupling of two imine motifs is observed (Scheme 29) [113]. A dimeric species of mixed valence is formed, suggesting that CO traps a reactive $[Ni^0]$ complex of **L4**. Therefore, the PPh_3 co-ligand plays an important role in stabilizing a reactive, monomeric species. By comparison, the related olefin complex **L2Ni^0** (Scheme 18) [88] features iPr-substituents on the phosphine linkers which give sufficient steric encumbrance to obtain monomeric species. In the case of the sterically less encumbered reactive $[Ni^0]$ species, however, dimerization and redox processes take place instead.

Bifunctional activation of a Si–H bond was observed upon reaction of **L4Ni^0(PPh$_3$)** with Ph_2SiH_2, resulting in hydrosilylation of the imine bond [114]. The hydrosilazane product (Scheme 30) was initially characterized by multinuclear NMR spectroscopy, revealing, interestingly, that the remaining Si–H bond is σ-coordinated to the Ni^0 center. This η^2(Si–H) coordination to the Ni center was confirmed in an X-ray crystal structure of a structurally analogous hydrosilazane compound resulting from the reaction of **L4Ni^0(PPh$_3$)** and phenyl-methylsilane ($PhMeSiH_2$; Fig. 21).

DFT calculations found a transition state for the Si–H bond activation in which the oxidative addition of the Si–H bond and the β-hydride insertion into the imine double bond to proceed in a concerted step (Scheme 30, middle). Therefore, a ligand-to-ligand hydride transfer mechanism is suggested, illustrating the ability of the imine ligand to facilitate bond activation processes by acting as a hydride acceptor moiety.

A relatively weak N–Si interaction as indicated by a relatively long N–Si distance (2.3266(5) Å) prompted an investigation into the reactivity of the hydrosilazane complex by means of silane scrambling experiments. Treatment of **L4Ni^0(PPh$_3$)** with deuterated diphenylsilane (Ph_2SiD_2) established a C–D bond in the ligand backbone, which does not exchange with the Si–H bonds of added hydrosilanes, indicating that hydrosilylation is irreversible. When exposed to phenyl-methylsilane ($PhMeSiH_2$; Scheme 31), the N–($SiPh_2D$) fragment is partially exchanged for N–($SiMePhH$) with concomitant formation of Ph_2SiHD, indicating facile and reversible cleavage of the N–Si bond. Hence, the system appears to convert from an initial stoichiometric hydride acceptor to a more reactive silyl reservoir by formal hydrosilylation of the π-acceptor imine motif. This suggests an intriguing strategy
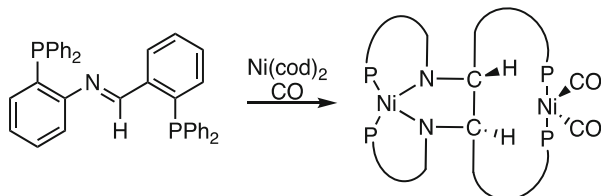
Scheme 29 Reaction of **L4** with a Ni⁰ precursor in the presence of CO gas leads to a dimeric species which is schematically drawn to emphasize the new C–C bond [113]
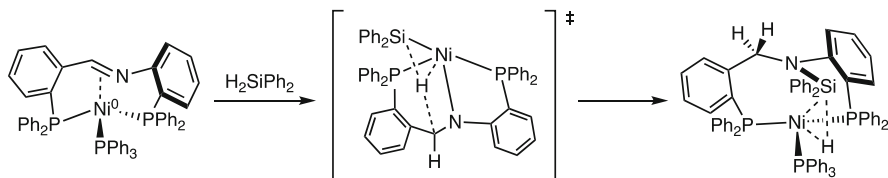
Scheme 30 Bifunctional Si–H bond activation by a **L4Ni⁰(PPh₃)** complex is thought to proceed through a concerted transition state via ligand-to-ligand hydride transfer [114]
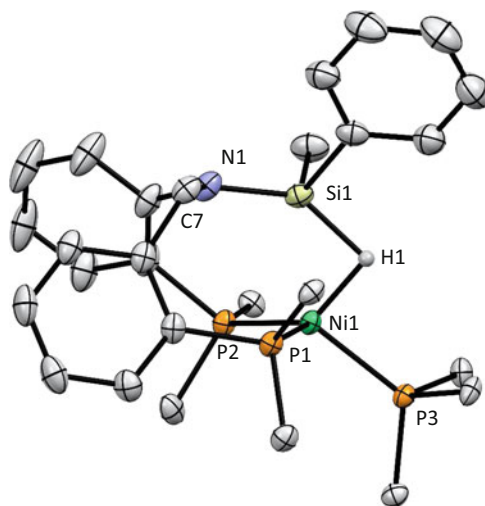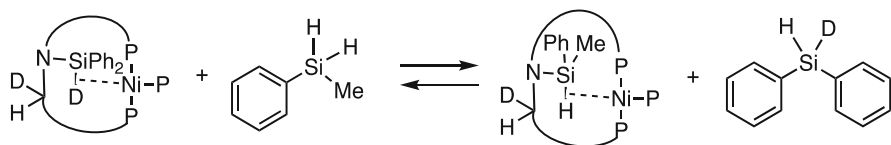

Fig. 21 X-ray crystal structure of the hydrosilazane complex showing the σ-coordinated Si-H bond (thermal ellipsoids at 50% probability). Hydrogen atoms (except the hydride) and phenyl groups on the phosphorus atoms (except for the bound carbon atoms) are omitted for clarity [114]

Scheme 31 Schematic representation of the silane scrambling experiment [114]

counter anion: $[SbF_6]^{\ominus}$
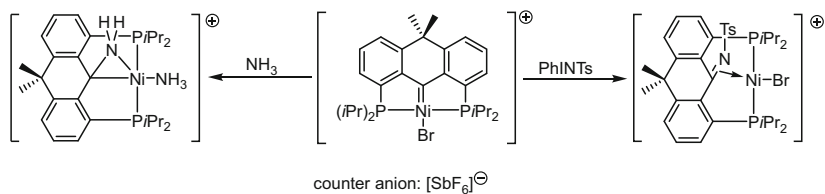
Scheme 32 Formation of a metalloaziridine Ni complex by reaction of a Ni carbene with NH_3 (left) and formation of a $\eta^2(C,N)$ bound imine motif by reaction of the Ni carbene with (tosylimino)-phenyl-$\lambda 3$-iodane (PhINTs) [115]

to generate reactive species by cooperative cleavage of element-hydrogen bonds using the **L3Ni^0(PPh$_3$)** or related acceptor pincer systems.

Apart from the presently discussed example, metal-ligand cooperative systems employing a π-acceptor imine pincer ligand are scarce. This is likely due to the propensity of imine ligands to form $\eta^1(N)$ complexes, requiring subtle ligand design. As mentioned before, side-on coordinated ketone motifs can be synthesized in the coordination sphere of a transition metal by formal oxygen atom transfer processes to a carbene complex. Similar reactivity was observed by Piers and co-workers who reported on a Ni carbene complex which upon reaction with (tosylimino)phenyl-$\lambda 3$-iodane (PhINTs) forms a new imine bond (Scheme 32, right) [115]. The imine double bond has a bond length of 1.354(4) Å, indicating a strong coordination of the imine to Ni. The coordination resembles the metallacycle extreme of the DCD model.

While reaction with PhINTs leads to a new π-complex, reaction of the Ni carbene with ammonia (NH_3) leads to a protonated metalloaziridine (Scheme 32, left). The product features a new C–N single bond (1.440(4) Å) which is with a Ni–N distance of 2.050(3) Å in close proximity of the Ni center. This product formally arises from coordination of NH_3 to the carbene followed by deprotonation by a second equivalent of NH_3 and release of $[NH_4]Br$. A third NH_3 equivalent then occupies the empty coordination side at Ni. Contrary to the reported work on reductive deoxygenation of η^2 (C,O)-coordinated ketone complexes (Sect. 3.3), a reversible transformation between a carbene complex and the corresponding η^2 (C,N)-coordinated imine complex has not been established so far. Future research might be aimed at investigating this possibility as well as the general proposed ability of the imine to act as hydride relay.

4 Concluding Remarks

The majority of pincer complexes, featuring a strong donor ligand in the central position, behave as a rigid ligand framework. In contrast, the incorporation of a central σ- or π-acceptor motif affords more flexible pincer ligands, giving access to a variety of different binding modes originating from the – generally weak – metal-

acceptor ligand interaction. Besides the different symmetry of the accepting orbital, a significant difference between σ- and π-acceptors is the necessary presence, in the latter, of a (weakly) donating π orbital that contributes to the bonding to the transition metal. As a consequence, σ-acceptor motifs are likely more electron-withdrawing than π-acceptors and hence may have a stronger impact on the electronic properties (e.g., Lewis acidity) of the transition metal. On the other hand, π-acceptors open a wide spectrum of opportunities for metal-ligand cooperation due to the accessibility of related structures such as vinyl- (C=C) and carbene species (C = E, E = C, N, O) and to the presence of additional lone pairs (π-ketone and π-imine).

In recent years, the field of acceptor pincer ligands has expanded rapidly from reports on unique coordination behavior and studies on stoichiometric cooperative reactivity to catalytic examples demonstrating the value and potential of the different classes of cooperative acceptor ligands for homogeneous catalysis. The "inverted" polarity of the metal-acceptor interaction manifests itself in two main classes of cooperative processes.

First, the accessible empty orbital can reversibly accept electron density (hemilability), increasing the range of electronic structures accessible to a given transition metal center. This adaptive coordination can be expanded further with the participation of neighboring groups, such as boron-bound aromatic residues or with alternative (donor) binding modes such as the $\eta^1(N)$ mode for imines. This flexibility allows both σ- and π-acceptor ligands to stabilize transition metal centers in a range of formal oxidation states and possibly facilitate (formal) redox processes. In particular, the hemilabile coordination behavior of a π-acceptor ketone motif (L3) has an accelerating effect in the alkyne cyclotrimerization reaction catalyzed by **L3Ni⁰(BPI)** [100, 101].

Second, the empty orbital can reversibly accept a nucleophilic fragment, which is frequently a hydride (bifunctional activity). Distinct reactivity pathways occur upon hydride uptake by either σ- or π-acceptor ligands: the former often acts as hydride acceptor by hydride insertion to form a bridging **L1-H-TM** motif, while the latter undergoes β-hydride insertion to reduce the π-bond. Both of these processes have been observed in the stoichiometric activation of H–H and E–H (E = Si, C, N, O, etc.) bonds. Furthermore, such hydride insertions are a crucial step in two examples of cooperative catalysis discussed in this chapter, namely, the catalytic hydrodechlorination of (hetero)aryl chlorides by the σ-acceptor pincer complex **L1Pd⁰(PPh₃)** [70] and reductive deoxygenation of amine and pyridine *N*-oxides catalyzed by the π-acceptor complex **[L3Rhᴵ(PPh₃)][BArᶠ₄]** [107]. In this way, both cooperative hydride uptake mechanisms have their specific impact. Future work exploiting the ability of acceptor ligands to transiently accept a hydride or other nucleophiles for substrate activation and catalysis is eagerly awaited.

In general, the correlation between acceptor pincer ligand coordination and cooperative (catalytic) reactivity of the metal complex constitutes an exciting area for discovery of bond activation processes and catalytic reactions using metal-ligand cooperation.

References

1. Karunananda MK, Mankad NP (2017) Cooperative strategies for catalytic hydrogenation of unsaturated hydrocarbons. ACS Catal 7:6110–6119
2. Khusnutdinova JR, Milstein D (2015) Metal–ligand cooperation. Angew Chem Int Ed 54:12236–12273
3. Balaraman E, Gunanathan C, Zhang J, Shimon LJW, Milstein D (2011) Efficient hydrogenation of organic carbonates, carbamates and formates indicates alternative routes to methanol based on CO2 and CO. Nat Chem 3:609–614
4. Semproni SP, Milsmann C, Chirik PJ (2014) Four-coordinate cobalt pincer complexes: electronic structure studies and ligand modification by Homolytic and Heterolytic pathways. J Am Chem Soc 136:9211–9224
5. Shvo Y, Czarkie D, Rahamim Y, Chodosh DF (1986) A new group of ruthenium complexes: structure and catalysis. J Am Chem Soc 108:7400–7402
6. Langer R, Leitus G, Ben-David Y, Milstein D (2011) Efficient hydrogenation of ketones catalyzed by an iron pincer complex. Angew Chem Int Ed 50:2120–2124
7. Chirik PJ (2011) Preface: forum on redox-active ligands. Inorg Chem 50:9737–9740
8. Chirik PJ, Wieghardt K (2010) Radical ligands confer nobility on base-metal catalysts. Science 327:794
9. Arevalo R, Chirik PJ (2019) Enabling two-electron pathways with Iron and cobalt: from ligand design to catalytic applications. J Am Chem Soc 141:9106–9123
10. Dzik WI, van der Vlugt JI, Reek JNH, de Bruin B (2011) Ligands that store and release electrons during catalysis. Angew Chem Int Ed 50:3356–3358
11. Luca OR, Crabtree RH (2013) Redox-active ligands in catalysis. Chem Soc Rev 42:1440–1459
12. Myers TW, Berben LA (2013) Aluminum–ligand cooperative N–H bond activation and an example of dehydrogenative coupling. J Am Chem Soc 135:9988–9990
13. Myers TW, Kazem N, Stoll S, Britt RD, Shanmugam M, Berben LA (2011) A redox series of aluminum complexes: characterization of four oxidation states including a ligand Biradical state stabilized via exchange coupling. J Am Chem Soc 133:8662–8672
14. van der Vlugt JI (2012) Cooperative catalysis with first-row late transition metals. Eur J Inorg Chem 2012:363–375
15. Braunstein P, Naud F (2001) Hemilability of hybrid ligands and the coordination chemistry of oxazoline-based systems. Angew Chem Int Ed 40:680–699
16. Jeffrey JC, Rauchfuss TB (1979) Metal complexes of hemilabile ligands. Reactivity and structure of dichlorobis(o-(diphenylphosphino)anisole)ruthenium(II). Inorg Chem 18:2658–2666
17. Adams GM, Weller AS (2018) POP-type ligands: variable coordination and hemilabile behaviour. Coord Chem Rev 355:150–172
18. Lindner R, van den Bosch B, Lutz M, Reek JNH, van der Vlugt JI (2011) Tunable hemilabile ligands for adaptive transition metal complexes. Organometallics 30:499–510
19. van der Vlugt JI, Pidko EA, Vogt D et al (2008) T-shaped cationic CuI complexes with hemilabile PNP-type ligands. Inorg Chem 47:4442–4444
20. van der Vlugt JI, Pidko EA, Vogt D, Lutz M, Spek AL, Meetsma A (2009) CuI complexes with a noninnocent PNP ligand: selective dearomatization and electrophilic addition reactivity. Inorg Chem 48:7513–7515

21. Noyori R (2002) Asymmetric catalysis: science and opportunities (Nobel lecture). Angew Chem Int Ed 41:2008–2022
22. Lawrence MAW, Green K-A, Nelson PN, Lorraine SC (2018) Review: pincer ligands – tunable, versatile and applicable. Polyhedron 143:11–27
23. Hetterscheid DGH, van der Vlugt JI, de Bruin B, Reek JNH (2009) Water splitting by cooperative catalysis. Angew Chem Int Ed 48:8178–8181
24. Bouhadir G, Bourissou D (2017) Coordination of Lewis acids to transition metals: Z-type ligands. In: Mingos DMP (ed) The chemical bond III: 100 years old and getting stronger. Springer, Cham, pp 141–201
25. Amgoune A, Bourissou D (2011) σ-acceptor, Z-type ligands for transition metals. Chem Commun 47:859–871
26. You D, Gabbaï FP (2019) Tunable σ-accepting, Z-type ligands for organometallic catalysis. Trends Chem 1:485–496
27. Owen GR (2016) Functional group migrations between boron and metal centres within transition metal–borane and –boryl complexes and cleavage of H–H, E–H and E–E' bonds. Chem Commun 52:10712–10726
28. Braunschweig H, Dewhurst RD (2011) Transition metals as Lewis bases: "Z-type" boron ligands and metal-to-boron dative bonding. Dalton Trans 40:549–558
29. Kameo H, Nakazawa H (2013) Recent developments in the coordination chemistry of multidentate ligands featuring a boron moiety. Chem Asian J 8:1720–1734
30. Verhoeven DGA, Moret M-E (2016) Metal–ligand cooperation at tethered π-ligands. Dalton Trans 45:15762–15778
31. Bouhadir G, Bourissou D (2016) Complexes of ambiphilic ligands: reactivity and catalytic applications. Chem Soc Rev 45:1065–1079
32. van Koten G, Timmer K, Noltes JG, Spek AL (1978) A novel type of Pt–C interaction and a model for the final stage in reductive elimination processes involving C–C coupling at Pt; synthesis and molecular geometry of [1,N,N'-η-2,6-bis{(dimethylamino)methyl}-toluene] iodoplatinum(II) tetrafluoroborate. J Chem Soc Chem Commun:250–252
33. Choi J, MacArthur AHR, Brookhart M, Goldman AS (2011) Dehydrogenation and related reactions catalyzed by iridium pincer complexes. Chem Rev 111:1761–1779
34. Albrecht M, van Koten G (2001) Platinum group organometallics based on "pincer" complexes: sensors, switches, and catalysts. Angew Chem Int Ed 40:3750–3781
35. Kirchner K (2015) Pincer and pincer-type complexes applications in organic synthesis and catalysis. Edited by Kálmán J. Szabó and Ola F. Wendt. Angew Chem Int Ed 54:4706–4707
36. Allen KE, Heinekey DM, Goldman AS, Goldberg KI (2013) Alkane dehydrogenation by C–H activation at iridium(III). Organometallics 32:1579–1582
37. Tanaka R, Yamashita M, Nozaki K (2009) Catalytic hydrogenation of carbon dioxide using Ir (III)−pincer complexes. J Am Chem Soc 131:14168–14169
38. Martín M, Sola E (2020) Chapter two – recent advances in the chemistry of group 9 – pincer organometallics. In: Pérez PJ (ed) Advances in organometallic chemistry. Academic Press, pp 79–193
39. Morales-Morales D (2018) Pincer compounds chemistry and applications. Elsevier, Amsterdam
40. Li H, Gonçalves TP, Lupp D, Huang K-W (2019) PN3(P)-pincer complexes: cooperative catalysis and beyond. ACS Catal 9:1619–1629
41. van Koten G, Milstein D (2013) Organometallic pincer chemistry. Springer, Berlin
42. Asay M, Morales-Morales D (2015) Non-symmetric pincer ligands: complexes and applications in catalysis. Dalton Trans 44:17432–17447
43. Lyaskovskyy V, de Bruin B (2012) Redox non-innocent ligands: versatile new tools to control catalytic reactions. ACS Catal 2:270–279
44. Gunanathan C, Milstein D (2011) Metal–ligand cooperation by aromatization–dearomatization: a new paradigm in bond activation and "Green" catalysis. Acc Chem Res 44:588–602

45. Schneider S, Meiners J, Askevold B (2012) Cooperative aliphatic PNP Amido pincer ligands – versatile building blocks for coordination chemistry and catalysis. Eur J Inorg Chem 2012:412–429
46. Alig L, Fritz M, Schneider S (2019) First-row transition metal (De)hydrogenation catalysis based on functional pincer ligands. Chem Rev 119:2681–2751
47. van der Vlugt JI, Reek JNH (2009) Neutral tridentate PNP ligands and their hybrid analogues: versatile non-innocent scaffolds for homogeneous catalysis. Angew Chem Int Ed 48:8832–8846
48. Budweg S, Junge K, Beller M (2020) Catalytic oxidations by dehydrogenation of alkanes, alcohols and amines with defined (non)-noble metal pincer complexes. Cat Sci Technol 10:3825–3842
49. Tondreau AM, Atienza CCH, Weller KJ, Nye SA, Lewis KM, Delis JGP, Chirik PJ (2012) Iron catalysts for selective anti-Markovnikov alkene hydrosilylation using tertiary silanes. Science 335:567
50. Green MLH (1995) A new approach to the formal classification of covalent compounds of the elements. J Organomet Chem 500:127–148
51. Hill AF, Owen GR, White AJP, Williams DJ (1999) The sting of the scorpion: a metallaboratrane. Angew Chem Int Ed 38:2759–2761
52. Bontemps S, Bouhadir G, Gu W, Mercy M, Chen CH, Foxman BM, Maron L, Ozerov OV, Bourissou D (2008) Metallaboratranes derived from a triphosphanyl–borane: intrinsic C3 symmetry supported by a Z-type ligand. Angew Chem Int Ed 47:1481–1484
53. Bourissou D, Bouhadir G (2016) Ambiphilic ligands: unusual coordination and reactivity arising from Lewis acid moieties. In: Stradiotto M, Lundgren RJ (eds) Ligand design in metal chemistry: reactivity and catalysis. Wiley, New York, pp 237–269
54. Bontemps S, Bouhadir G, Dyer PW, Miqueu K, Bourissou D (2007) Quasi-Thermoneutral P → B interactions within Di- and tri-phosphine boranes. Inorg Chem 46:5149–5151
55. Sircoglou M, Bontemps S, Bouhadir G et al (2008) Group 10 and 11 metal boratranes (Ni, Pd, Pt, CuCl, AgCl, AuCl, and Au+) derived from a triphosphine−borane. J Am Chem Soc 130:16729–16738
56. Bontemps S, Gornitzka H, Bouhadir G, Saffon N, Miqueu K, Gu W, Mercy M, Chen CH, Foxman BM, Maron L, Ozerov OV, Bourissou D (2006) Rhodium(I) complexes of a PBP ambiphilic ligand: evidence for a metal→borane interaction. Angew Chem Int Ed 45:1611–1614
57. Harman WH, Peters JC (2012) Reversible H2 addition across a nickel–borane unit as a promising strategy for catalysis. J Am Chem Soc 134:5080–5082
58. Sircoglou M, Bontemps S, Mercy M, Miqueu K, Ladeira S, Saffon N, Maron L, Bouhadir G, Bourissou D (2010) Copper(I) complexes derived from mono- and diphosphino-boranes: Cu→B interactions supported by arene coordination. Inorg Chem 49:3983–3990
59. Schindler T, Lux M, Peters M, Scharf LT, Osseili H, Maron L, Tauchert ME (2015) Synthesis and reactivity of palladium complexes featuring a diphosphinoborane ligand. Organometallics 34:1978–1984
60. Cao Y, Shih W-C, Bhuvanesh N, Ozerov OV (2019) Silver halide complexes of a borane/bis (phosphine) ligand. Dalton Trans 48:9959–9961
61. Sircoglou M, Bontemps S, Mercy M, Saffon N, Takahashi M, Bouhadir G, Maron L, Bourissou D (2007) Transition-metal complexes featuring Z-type ligands: agreement or discrepancy between geometry and dn configuration? Angew Chem Int Ed 46:8583–8586
62. Tauchert ME, Steinhoff P (2016) A T-shape diphosphinoborane palladium(0) complex. Beilstein J Org Chem 12:1573–1576
63. Inagaki F, Matsumoto C, Okada Y, Maruyama N, Mukai C (2015) Air-stable cationic gold (I) catalyst featuring a Z-type ligand: promoting enyne cyclizations. Angew Chem Int Ed 54:818–822
64. Murakami R, Inagaki F (2019) Recent topics of gold catalyst featuring Z-type ligands. Tetrahedron Lett 60:151231

65. Harman WH, Lin T-P, Peters JC (2014) A d10 Ni–(H2) adduct as an intermediate in H-H oxidative addition across a Ni-B bond. Angew Chem Int Ed 53:1081–1086
66. Li Y, Hou C, Jiang J, Zhang Z, Zhao C, Page AJ, Ke Z (2016) General H2 activation modes for Lewis acid–transition metal bifunctional catalysts. ACS Catal 6:1655–1662
67. MacMillan SN, Hill Harman W, Peters JC (2014) Facile Si–H bond activation and hydrosilylation catalysis mediated by a nickel–borane complex. Chem Sci 5:590–597
68. Schuhknecht D, Ritter F, Tauchert ME (2016) Isolation and properties of a palladium PBP pincer complex featuring an ambiphilic boryl site. Chem Commun 52:11823–11826
69. Shih W-C, Gu W, MacInnis MC, Timpa SD, Bhuvanesh N, Zhou J, Ozerov OV (2016) Facile insertion of Rh and Ir into a boron–phenyl bond, leading to Boryl/Bis(phosphine) PBP pincer complexes. J Am Chem Soc 138:2086–2089
70. Kameo H, Yamamoto J, Asada A, Nakazawa H, Matsuzaka H, Bourissou D (2019) Palladium–borane cooperation: evidence for an anionic pathway and its application to catalytic hydro-/deutero-dechlorination. Angew Chem Int Ed 58:18783–18787
71. Conifer CM, Law DJ, Sunley GJ, White AJP, Britovsek GJP (2011) Lewis acids and Lewis acid-functionalized ligands in rhodium-catalyzed methyl acetate carbonylation. Organometallics 30:4060–4066
72. Shih W-C, Gu W, MacInnis MC, Herbert DE, Ozerov OV (2017) Boryl/borane interconversion and diversity of binding modes of oxygenous ligands in PBP pincer complexes of rhodium. Organometallics 36:1718–1726
73. Kameo H, Nakazawa H (2012) Synthesis of a rhodium complex featuring the Rh–H–B linkage via a hydride migration from rhodium to borane: study on the electronic deviation induced by the presence of the boron moiety. Organometallics 31:7476–7484
74. Suess DLM, Peters JC (2013) H–H and Si–H bond addition to Fe≡NNR2 intermediates derived from N2. J Am Chem Soc 135:4938–4941
75. Suess DLM, Peters JC (2013) A CO-derived iron dicarbyne that releases olefin upon hydrogenation. J Am Chem Soc 135:12580–12583
76. Nesbit MA, Suess DLM, Peters JC (2015) E–H bond activations and hydrosilylation catalysis with iron and cobalt metalloboranes. Organometallics 34:4741–4752
77. Zeise WC (1827) Poggendorffs Annalen der Physik 9:632–633
78. Mingos DMP (2001) A historical perspective on Dewar's landmark contribution to organometallic chemistry. J Organomet Chem 635:1–8
79. Comanescu CC, Vyushkova M, Iluc VM (2015) Palladium carbene complexes as persistent radicals. Chem Sci 6:4570–4579
80. Comanescu CC, Iluc VM (2014) Synthesis and reactivity of a nucleophilic palladium (II) carbene. Organometallics 33:6059–6064
81. Gusev DG, Lough AJ (2002) Double C−H activation on osmium and ruthenium centers: carbene vs olefin products. Organometallics 21:2601–2603
82. Crocker C, Errington RJ, McDonald WS, Odell KJ, Shaw BL, Goodfellow RJ (1979) Rapid reversible fission of a C–H bond in a metal complex: X-ray crystal structure of [RhHCl (But2PCH2CH2CHCH2CH2PBut2)]. J Chem Soc Chem Commun:498–499
83. Vigalok A, Kraatz H-B, Konstantinovsky L, Milstein D (1997) Evidence for direct trans insertion in a Hydrido-olefin rhodium complex – free nitrogen as a trap in a migratory insertion process. Chem Eur J 3:253–260
84. Jonasson KJ, Polukeev AV, Marcos R, Ahlquist MSG, Wendt OF (2015) Reversible α-hydrogen and α-alkyl elimination in PC(sp3)P pincer complexes of iridium. Angew Chem Int Ed 54:9372–9375
85. Polukeev AV, Marcos R, Ahlquist MSG, Wendt OF (2015) Formation of a C–C double bond from two aliphatic carbons. Multiple C–H activations in an iridium pincer complex. Chem Sci 6:2060–2067
86. Polukeev AV, Wendt OF (2015) Iridium pincer complexes with an olefin backbone. Organometallics 34:4262–4271

87. Barrett BJ, Iluc VM (2014) Coordination of a hemilabile pincer ligand with an olefinic backbone to mid-to-late transition metals. Inorg Chem 53:7248–7259
88. Barrett BJ, Iluc VM (2014) Group 10 metal complexes supported by pincer ligands with an olefinic backbone. Organometallics 33:2565–2574
89. Bennett MA, Clark PW (1976) Tridentate chelate π-bonded complexes of rhodium(I), iridium (I), and iridium(III) and chelate σ-bonded complexes of nickel(II), palladium(II), and platinum (II) formed by intramolecular hydrogen abstraction reactions. J Organomet Chem 110:367–381
90. Baratta W, Herdtweck E, Martinuzzi P, Rigo P (2001) Carbon−carbon double bond formation from two o-methyl groups in osmium phosphine complexes. Organometallics 20:305–308
91. Campos J, Ortega-Moreno L, Conejero S, Peloso R, López-Serrano J, Maya C, Carmona E (2015) Reactivity of cationic Agostic and Carbene structures derived from platinum (II) metallacycles. Chem Eur J 21:8883–8896
92. Barrett BJ, Iluc VM (2017) Metal-ligand cooperation between palladium and a diphosphine ligand with an olefinic backbone. Inorg Chim Acta 460:35–42
93. Bennett MA, Johnson RN, Tomkins IB (1976) Additions to metal atom and to coordinated ligand in complexes of rhodium(I) and iridium(I) formed by a tridentate olefinic ditertiary phosphine: chelate olefin complexes and σ-alkyls of rhodium(III) and iridium(III). J Organomet Chem 118:205–232
94. Jing Q, Sandoval CA, Wang Z, Ding K (2006) Complete chiral induction from Enantiopure 1,2-diamines to benzophenone-based achiral Bisphosphane ligands in Noyori-type RuII catalysts. Eur J Org Chem 2006:3606–3616
95. Saes BWH, Verhoeven DGA, Lutz M, Klein Gebbink RJM, Moret ME (2015) Coordination of a diphosphine–ketone ligand to Ni(0), Ni(I), and Ni(II): reduction-induced coordination. Organometallics 34:2710–2713
96. Verhoeven DGA, van Wiggen MAC, Kwakernaak J, Lutz M, Klein Gebbink RJM, Moret ME (2018) Periodic trends in the binding of a phosphine-tethered ketone ligand to Fe, Co, Ni, and Cu. Chem Eur J 24:5163–5172
97. Sung S, Wang Q, Krämer T, Young RD (2018) Synthesis and reactivity of a PCcarbeneP cobalt(i) complex: the missing link in the cobalt PXP pincer series (X = B, C, N). Chem Sci 9:8234–8241
98. Rothstein PE, Comanescu CC, Iluc VM (2017) Formation of palladium η2-bound Chalcogenoketones across a Pd+−C− bond. Chem Eur J 23:16948–16952
99. Sung S, Boon JK, Lee JJC, Rajabi NA, Macgregor SA, Krämer T, Young RD (2017) Convergent (De)hydrogenative pathways via a rhodium α-hydroxylalkyl complex. Organometallics 36:1609–1617
100. Orsino AF, Gutiérrez del Campo M, Lutz M, Moret M-E (2019) Enhanced catalytic activity of nickel complexes of an adaptive diphosphine–benzophenone ligand in alkyne cyclotrimerization. ACS Catal 9:2458–2481
101. Orsino AF, Moret M-E (2020) Nickel-catalyzed alkyne cyclotrimerization assisted by a hemilabile acceptor ligand: a computational study. Organometallics 39:1998–2010
102. Sung S, Young RD (2017) Facile generation of iridium PCcarbeneP pincer complexes via water elimination from an alcohol proligand. Dalton Trans 46:15407–15414
103. Sung S, Joachim T, Krämer T, Young RD (2017) Protonolysis of an α-hydroxyl ligand for the generation of a PCcarbeneP pincer complex and subsequent reactivity studies. Organometallics 36:3117–3124
104. Doyle LE, Piers WE, Borau-Garcia J (2015) Ligand cooperation in the formal hydrogenation of N2O using a PCsp2P iridium pincer complex. J Am Chem Soc 137:2187–2190
105. Doyle LE, Piers WE, Borau-Garcia J, Sgro MJ, Spasyuk DM (2016) Mechanistic studies on the addition of hydrogen to iridaepoxide complexes with subsequent elimination of water. Chem Sci 7:921–931
106. Doyle LE, Piers WE, Bi DW (2017) Cationic PCP iridaepoxide and carbene complexes for facile water elimination and activation processes. Dalton Trans 46:4346–4354

107. Tinnermann H, Sung S, Cala BA, Gill HJ, Young RD (2020) Catalytic deoxygenation of amine and pyridine N-oxides using rhodium PCcarbeneP pincer complexes. Organometallics 39:797
108. Sung S, Tinnermann H, Krämer T, Young RD (2019) Direct oxide transfer from an η2-keto ligand to generate a cobalt PCcarbeneP(O) pincer complex. Dalton Trans 48:9920–9924
109. Ainscough EW, Brodie AM, Buckley PD, Burrell AK, Kennedy SMF, Waters JM (2000) Synthesis, structure and kinetics of group 6 metal carbonyl complexes containing a new 'P2N' mixed donor multidentate ligand. J Chem Soc Dalton Trans:2663–2671
110. Hou J, Sun WH, Zhang S, Ma H, Deng Y, Lu X (2006) Synthesis and characterization of tridentate nickel complexes bearing P∧N∧N and P∧N∧P ligands and their catalytic property in ethylene oligomerization. Organometallics 25:236–244
111. Chen L, Ai P, Gu J, Jie S, Li BG (2012) Stereospecific polymerization of 1,3-butadiene catalyzed by cobalt complexes bearing N-containing diphosphine PNP ligands. J Organomet Chem 716:55–61
112. Doherty S, Knight JG, Scanlan TH, Elsegood MRJ, Clegg W (2002) Iminophosphines: synthesis, formation of 2,3-dihydro-1H-benzo[1,3]azaphosphol-3-ium salts and N-(pyridin-2-yl)-2-diphenylphosphinoylaniline, coordination chemistry and applications in platinum group catalyzed Suzuki coupling reactions and hydrosilylations. J Organomet Chem 650:231–248
113. Verhoeven DGA, Negenman HA, Orsino AF, Lutz M, Moret ME (2018) Versatile coordination and C–C coupling of diphosphine-tethered imine ligands with Ni(II) and Ni(0). Inorg Chem 57:10846–10856
114. Verhoeven DGA, Orsino AF, Bienenmann RLM, Lutz M, Moret ME (2020) Cooperative Si–H addition to side-on Ni(0)-imine complexes forms reactive hydrosilazane complexes. Organometallics 39:623–629
115. LaPierre EA, Piers WE, Gendy C (2018) Redox-state dependent activation of silanes and ammonia with reverse polarity (PCcarbeneP)Ni complexes: electrophilic vs. nucleophilic carbenes. Dalton Trans 47:16789–16797